The 2020 COVID-19 pandemic and atmospheric composition: back to the future

Joshua L. Laughner[1], Jessica L. Neu[2], David Schimel[2], Paul O. Wennberg[3], Kelley Barsanti[4], Kevin Bowman[2], Abhishek Chatterjee[5], Bart Croes[6], Helen Fitzmaurice[7], Daven Henze[8], Jinsol Kim[7], Eric A. Kort[9], Zhu Liu[10], Kazuyuki Miyazaki[11], Alexander J. Turner[12], Susan Anenberg[13], Jeremy Avise[14], Hansen Cao[15], David Crisp[2], Joost de Gouw[16], Annmarie Eldering[2], John C. Fyfe[17], Daniel L. Goldberg[13], Kevin R. Gurney[18], Sina Hasheminassab[19], Francesca Hopkins[20], Cesunica E. Ivey[21], Dylan B.A. Jones[22], Nicole S. Lovenduski[23], Randall V. Martin[24], Galen A. McKinley[25], Lesley Ott[26], Benjamin Poulter[27], Muye Ru[28], Stanley P. Sander[2], Neil Swart[17], Yuk L. Yung[3], and Zhao-Cheng Zeng[29]

[1]Division of Geological and Planetary Sciences California Institute of Technology
[2]Jet Propulsion Laboratory California Institute of Technology
[3]Division of Geological and Planetary Sciences California Institute of Technology
[4]Department of Chemical and Environmental Engineering - Marlan and Rosemary Bourns College of Engineering University of California Riverside
[5]Universities Space Research Association
[6]California Energy Commission
[7]Department of Earth and Planetary Science University of California Berkeley
[8]Department of Mechanical Engineering University of Colorado at Boulder
[9]Department of Climate and Space Sciences and Engineering University of Michigan
[10]Department of Earth System Science Tsinghua University
[11]Jet Propulsion Laboratory, California Institute of Technology
[12]Department of Atmospheric Sciences University of Washington
[13]Milken Institute School of Public Health George Washington University
[14]Modeling and Meteorology Branch California Air Resources Board
[15]Department of Mechanical Engineering University of Colorado at Boulder
[16]Department of Chemistry and Cooperative Institute for Research in Environmental Sciences University of Colorado Boulder
[17]Canadian Centre for Climate Modelling and Analysis Environment and Climate Change Canada
[18]School of Informatics - Computing and Cyber Systems Northern Arizona University
[19]Science and Technology Advancement Division South Coast Air Quality Management District
[20]Department of Environmental Sciences University of California, Riverside
[21]Department of Chemical and Environmental Engineering - Marlan and Rosemary Bourns College of Engineering University of California Riverside
[22]Department of Physics University of Toronto
[23]Department of Atmospheric and Oceanic Sciences and Institute of Arctic and Alpine

Posted on 30 Nov 2022 — CC-BY-NC-ND 4 — https://doi.org/10.1002/essoar.10506081/v1 — This a preprint and has not been peer reviewed. Data may be preliminary.

Research University of Colorado Boulder
[24]McKelvey School of Engineering Washington University in St. Louis
[25]Department of Earth and Environmental Sciences Columbia University
[26]Global Modeling and Assimilation Office NASA Goddard Space Flight Center
[27]Biospheric Sciences Laboratory NASA GSFC Goddard Space Flight Center
[28]The Earth Institute Columbia University
[29]Joint Institute for Regional Earth System Science and Engineering University of California, Los Angeles

November 30, 2022

Abstract

The COVID-19 global pandemic and associated government lockdowns dramatically altered human activity, providing a window into how changes in individual behavior, enacted en masse, impact atmospheric composition. The resulting reductions in anthropogenic activity represent an unprecedented event that yields a glimpse into both the past and a future where emissions to the atmosphere are reduced. While air pollutants and greenhouse gases share many common anthropogenic sources, there is a sharp difference in the response of their atmospheric concentrations to COVID-19 emissions changes due in large part to their different lifetimes. Here, we discuss the lessons learned from the COVID-19 disruptions for future mitigation strategies and our current and future Earth observing system.

Posted on 30 Nov 2022 — CC-BY-NC-ND 4 — https://doi.org/10.1002/essoar.10506081/v1 — This a preprint and has not been peer reviewed. Data may be preliminary.

The 2020 COVID-19 pandemic and atmospheric composition: back to the future

Joshua L. Laughner[a,1], Jessica L. Neu[b,1], David Schimel[b,1], Paul O. Wennberg[a,c,1], Kelley Barsanti[d], Kevin Bowman[b], Abhishek Chatterjee[e,f], Bart Croes[g,o], Helen Fitzmaurice[h], Daven Henze[i], Jinsol Kim[h], Eric A. Kort[j], Zhu Liu[k], Kazuyuki Miyazaki[b], Alexander J. Turner[l,h,b], Susan Anenberg[m], Jeremy Avise[n], Hansen Cao[i], David Crisp[b], Joost de Gouw[o], Annmarie Eldering[b], John C. Fyfe[p], Daniel L. Goldberg[m], Kevin R. Gurney[q], Sina Hasheminassab[r], Francesca Hopkins[s], Cesunica E. Ivey[d,t], Dylan B.A. Jones[u], Nicole S. Lovenduski[v], Randall V. Martin[w], Galen A. McKinley[x], Lesley Ott[y], Benjamin Poulter[z], Muye Ru[aa], Stanley P. Sander[b], Neil Swart[p], Yuk L. Yung[a,b], Zhao-Cheng Zeng[bb], and the rest of the Keck Institute for Space Studies "COVID-19: Identifying Unique Opportunities for Earth System Science" study team[1]

[a]Division of Geological and Planetary Sciences, California Institute of Technology; [b]Jet Propulsion Laboratory, California Institute of Technology; [c]Division of Engineering and Applied Science, California Institute of Technology; [d]Department of Chemical and Environmental Engineering, Marlan and Rosemary Bourns College of Engineering, University of California, Riverside, CA 92521, United States; [e]Universities Space Research Association, Columbia, MD 21046, United States; [f]NASA Goddard Space Flight Center, Greenbelt, MD 20771, United States; [g]California Energy Commission, Sacramento, CA 95814, United States; [h]Department of Earth and Planetary Science, University of California, Berkeley, Berkeley, CA 94720, USA; [i]Department of Mechanical Engineering, University of Colorado at Boulder, Boulder, CO 80309 United States; [j]Department of Climate and Space Sciences and Engineering, University of Michigan, Ann Arbor, Michigan 48109, United States; [k]Department of Earth System Science, Tsinghua University, Beijing 100084, China; [l]Department of Atmospheric Sciences, University of Washington, Seattle, WA 98195, United States; [m]Milken Institute School of Public Health, George Washington University, Washington, DC 20052, United States; [n]Modeling and Meteorology Branch, California Air Resources Board, Sacramento, CA 95814, United States; [o]Department of Chemistry and Cooperative Institute for Research in Environmental Sciences, University of Colorado Boulder, Boulder, CO 80309, USA; [p]Canadian Centre for Climate Modelling and Analysis, Environment and Climate Change Canada, Victoria, BC, Canada; [q]School of Informatics, Computing and Cyber Systems, Northern Arizona University, Flagstaff, AZ 86011, United States; [r]Science and Technology Advancement Division, South Coast Air Quality Management District, Diamond Bar, CA, 91765, USA; [s]Department of Environmental Sciences, University of California, Riverside, California, USA; [t]Center for Environmental Research and Technology, Riverside, CA 92521, United States; [u]Department of Physics, University of Toronto, Toronto, Ontario, Canada; [v]Department of Atmospheric and Oceanic Sciences and Institute of Arctic and Alpine Research, University of Colorado, Boulder, CO, USA; [w]McKelvey School of Engineering, Washington University in St. Louis, St. Louis, Missouri 63130, United States; [x]Department of Earth and Environmental Sciences, Columbia University, Lamont Doherty Earth Observatory, Palisades, NY 10964, United States; [y]Global Modeling and Assimilation Office, NASA Goddard Space Flight Center, Greenbelt, MD, United States; [z]Biospheric Sciences Laboratory, NASA GSFC Goddard Space Flight Center, MD, United States; [aa]The Earth Institute, Columbia University, New York, NY 10025, United States; [bb]Joint Institute for Regional Earth System Science and Engineering, University of California, Los Angeles, CA 90095, United States

This manuscript was compiled on February 3, 2021

The COVID-19 global pandemic and associated government lockdowns dramatically altered human activity, providing a window into how changes in individual behavior, enacted *en masse*, impact atmospheric composition. The resulting reductions in anthropogenic activity represent an unprecedented event that yields a glimpse into both the past and a future where emissions to the atmosphere are reduced. While air pollutants and greenhouse gases share many common anthropogenic sources, there is a sharp difference in the response of their atmospheric concentrations to COVID-19 emissions changes due in large part to their different lifetimes. Here, we discuss the lessons learned from the COVID-19 disruptions for future mitigation strategies and our current and future Earth observing system.

COVID-19 | air quality | greenhouse gases | Earth system | mitigation

The effects of the COVID-19 pandemic and associated lockdown measures can be conceptualized as in Fig. 1. Changes in human activity led to rapid decreases in emissions; these changes can be thought of as going either backward in time to former anthropogenic emissions levels or forward in time to a set of emissions targets. However, because the emissions changes were rapid, the response of air quality and the carbon cycle are observable and can be used to inform effective mitigation strategies. Early estimates of carbon dioxide (CO_2) emissions changes suggest a total reduction for 2020 of about 7% (1, 2). Despite significant changes in individual behavior, this equates to moving back only to 2011 emission levels (Fig. 2a). Global nitrogen oxide (NO_x) emissions decreased to approximately 1999 levels, but this simple picture is complicated by the fact that the distribution of NO_x sources has changed significantly since that time. NO_x emissions have been decreasing for several decades in the US (3–7), since the mid-2000s in Europe (3, 7–9), and approximately seven to nine years in China (3, 5, 7, 10). In these regions, the impact of COVID-19 on air quality may be better thought of as jumping ahead in time to a period with stricter emissions controls (Fig. 2b). In countries whose NO_x emissions have been increasing, the emissions shifted as far back as 2008. The magnitude and even sign of COVID-related methane (CH_4) emission changes is currently unknown (Fig.2a) and is complicated by competing effects such as increases in oil and gas storage and decreases in maintenance activities.

Our goal, outlined in Fig. 1, is to present a first look at how the change in human activity during the COVID-19 pandemic led to reduced emissions, and in turn how air quality and the carbon cycle responded to this rapid change. We present lessons learned in how we might achieve the same level of

Significance Statement

The COVID-19 pandemic and associated lockdowns caused significant changes to human activity that temporarily altered our imprint on the atmosphere, providing a brief glimpse of both past and future atmospheric composition. This event showed key differences in how air quality and atmospheric greenhouse gas concentrations respond to changes in anthropogenic emissions, with implications for future mitigation strategies.

JLL lead the manuscript and the human activity analysis. JN, DS, and POW lead the study team. K. Barsanti, K. Bowman, DS, AT, and EK lead study subgroups and paper sections. AC, BC, HF, DH, JK, ZL, and KM also lead paper sections. Remaining authors contributed data analysis or text. All authors helped revise the manuscript.

The authors declare no competing interests.

[1]To whom correspondence should be addressed. E-mail: jlaugh@caltech.edu, jessica.l.neu@jpl.nasa.gov, david.schimel@jpl.nasa.gov, or wennberg@gps.caltech.edu

DRAFT

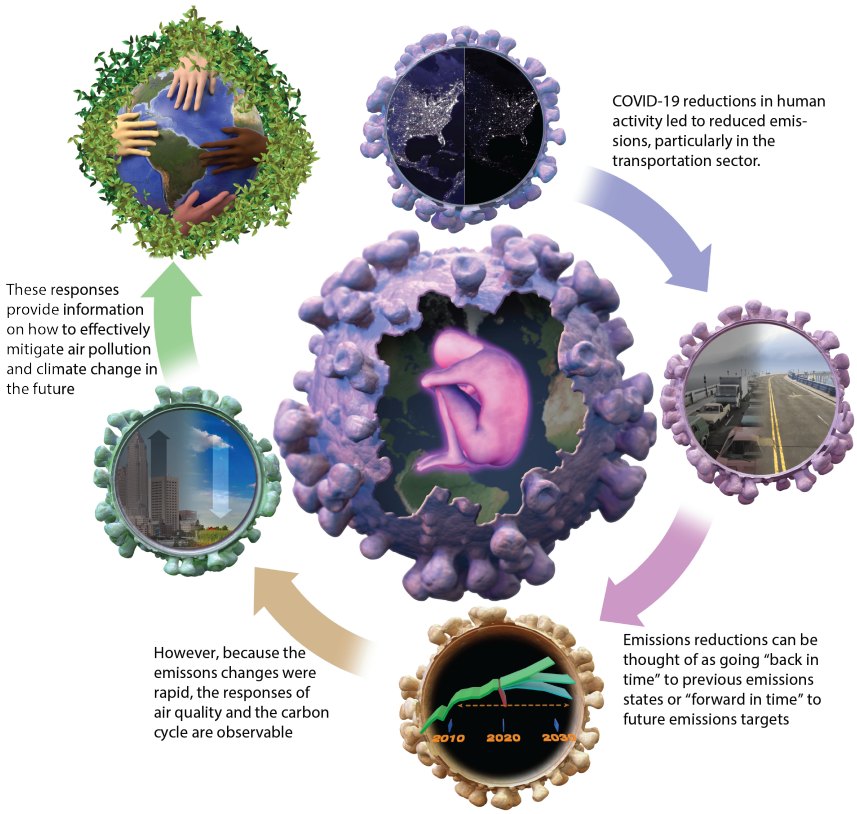

Fig. 1. Illustration of the conceptual flow of this study. The COVID-19-induced reductions in human activity led to reduced anthropogenic emissions. That shift, equivalent to moving forward or backward in time, shows us how the atmosphere, land, and ocean respond in a future scenario with stricter emissions controls. This analysis helps to identify pathways to mitigate air pollution and climate change without tremendous sacrifice from individuals. Image credit: Chuck Carter / Keck Institute for Space Studies

reduced emissions in the future without relying on tremendous individual sacrifice. This paper is organized in three parts. First, we describe the changes in human behavior that occurred during the pandemic. Second, we discuss the implications of observed changes in emissions and concentrations for future mitigation strategies, with special attention to how local-scale changes (using the San Francisco Bay Area and the Los Angeles Basin as case studies) collectively affect global climate and global-scale observations support strategies to improve local air quality. Finally, we examine what the COVID-19 pandemic has taught us about future needs for an Earth observing system and future lines of research.

1. Change in human activity during lockdowns

To place the atmospheric effects of the pandemic in context, we first need to understand how human activity changed. Figure 3 shows metrics for the strictness of government lockdown measures, vehicle traffic, air traffic, shipping, and electricity use. To highlight connections between the local and global scales, we include metrics focused specifically on two California urban areas (the San Francisco Bay Area and Los Angeles Basin), the US and other countries as a whole, and the world.

Except in China, vehicle traffic and air travel all show similar patterns of a sharp decrease in mid-March (Fig. 3b,c), when lockdowns and other protective measures went into effect in most locations (Fig. 3a), followed by a slow recovery over the following months. While California urban areas remained near or below their pre-pandemic traffic levels throughout the boreal summer, driving mobility throughout the whole US as reported by Apple increased nearly 200% between January and July. The Apple mobility data was only made available for 2020, so it is not possible to determine whether this represents a typical seasonal cycle in travel. Chinese air travel shows an earlier decrease and recovery than other locations, consistent with an earlier lockdown (Fig. 3a,b). Shipping at the Ports of Los Angeles (LA) and Long Beach showed a decrease in total container moves in February and March relative to January, while the Port of Oakland that serves the San Francisco Bay Area was less affected (Fig. 3b). In April and May, residential electricity use was higher in 2020 than 2019 across the US, while industrial and commercial use was lower (Fig. 3c,d). Total electricity use across all sectors in 2020 was about 5% lower than in 2019.

Taken together, these metrics paint a picture of disruption focused on specific sectors of activity associated with government policies to restrict peoples' movement. Thus, as an experiment, the COVID-19 pandemic and associated lockdowns primarily represent a test of the atmospheric response to emissions from passenger vehicles and airline travel.

2. Observed changes in air quality and implications for mitigation strategies

Air quality Observations. The COVID-19 lockdown measures led to a clear and rapid decrease in NO_x emissions (15, 16), providing a glimpse of the past for many countries but also a look ahead to the future under consistent, long-term emissions

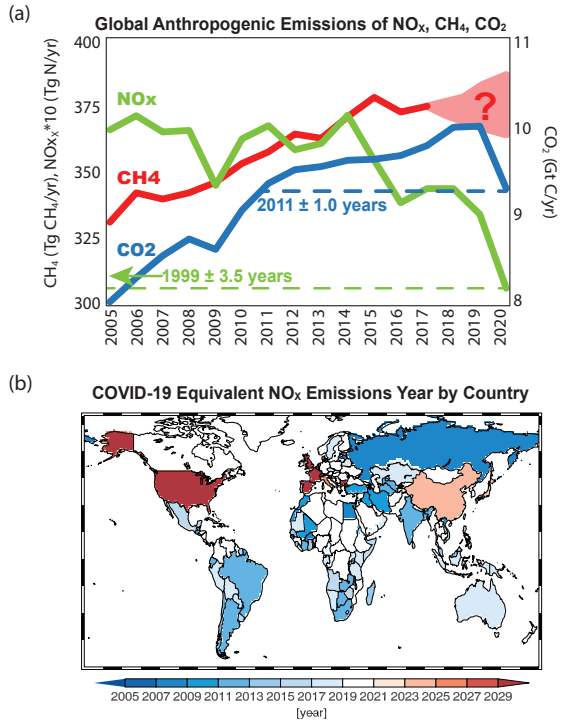

Fig. 2. **(a)** Time series of global NO_x, CH_4, and CO_2 emissions. For CO_2 and NO_x, the decrease due to COVID-19 is annotated with the year in the past that had equivalent global emissions to 2020. The effects of COVID-19 on CH_4 emissions is currently unknown. **(b)** Countries colored by the year to which their 2020 NO_x emissions are equivalent, projected forward in time where emissions have been decreasing and backward elsewhere. Details of emissions estimates given in the SI.

reduction policies (Fig. 2b). To understand the effects on these reductions on air quality (AQ), we begin with a comparison of AQ changes in different parts of the world, followed by a detailed look at the city of LA as an example of urban-scale effects. Figure 4, panels (a) through (c) show TROPOMI NO_2 columns for three megacities: Los Angeles, USA; Lima, Peru; and Shanghai, China. Compared to 2019, NO_2 levels are substantially lower in 2020 in these cities after lockdown measures were in place. However, the relationship between NO_2 column measurements and NO_x emissions, as well as the response of secondary pollutants to changes in NO_x, depend on a number of factors including time of year, meteorology, and chemistry; we use statistical (15) and data assimilation techniques that account for these factors to draw inferences about atmospheric composition changes from the satellite measurements.

Changes in NO_x emissions alter concentrations of secondary pollutants through shifts in photochemistry. Over highly polluted urban areas with high NO_x concentrations, reducing NO_x can increase ozone (O_3) production by attenuating the removal of OH and increasing volatile organic carbon (VOC) oxidation, particularly during winter (17). In lower NO_x environments, reducing NO_x can reduce O_3 production by slowing photochemistry. Additionally, lower NO_x concentrations mean less NO is available to convert O_3 to NO_2. Thus, the impact of COVID-19-induced emissions reductions on O_3 levels is highly contextual. The response of particulate matter (PM) levels to NO_x emissions reductions are likewise highly dependent on local sources and chemistry (18).

One major source of uncertainty in the responses of secondary pollutants to the COVID-19 lockdown measures is the associated changes in anthropogenic VOC emissions, for which we do not currently have good observational constraints. Gasoline-powered vehicles are important sources of VOCs in urban environments, and there were undoubtedly decreases in alkanes, alkenes and aromatics from passenger vehicle traffic. In that sense, the COVID-19 lockdowns are fundamentally different from weekend-weekday differences, which are primarily driven by decreases in NO_x-dominant diesel traffic. In addition, personal care and cleaning products have become important sources of VOCs in urban air (19), and the emissions changes associated with changes in the use of these products during COVID-19 are largely unknown.

Assuming climatological VOC emissions, an assimilation system constrained primarily by satellite NO_2 column observations (20) shows that O_3 production efficiencies (OPEs, defined as the change in tropospheric O_3 mass divided by the change in NO_x emissions) shifted in response to the COVID NO_x emissions reductions, with the change in OPE being highly variable in space and time. Figure 4d shows the February to June average OPE for 20 megacities around the globe. Los Angeles and Shanghai both have small positive OPEs, indicating that ozone did decrease in response to NO_x reductions seen in Figs. 4a and c, but that it is overall not very sensitive NO_x during boreal winter and spring. Further analysis of the Los Angeles Basin is provided below. Small and even negative OPE values (i.e. an increase in O_3 production per unit NO_x decrease) are found for most mid- and high- latitude cities for this time period. In contrast, the OPE for Lima is positive and large (3.5), indicating a strong sensitivity of ozone to the NO_x reductions in Fig. 4b. The large values of OPE for cities in tropical developing countries are associated with active photochemistry and efficient vertical transport from the surface into the entire troposphere.

OPE values also vary in time, driven largely by seasonal changes in incoming solar radiation. The mean OPE values averaged over the 20 megacities globally are relatively constant, ranging between 0.7 and 1.2. These global OPE values primarily reflect the large OPEs in the tropics and southern hemisphere subtropics (Fig. 4e), where seasonal changes in irradiance are small. The median OPE values over the northern hemisphere extratropical megacities, however, increase from 0.12 in February to 0.27 in June due to more active photochemistry as the midlatitudes transitioned from winter to summer (Fig. 4f).

Spatial variations in O_3 production associated with reduced NO_x emissions are seen not only globally, but also within a single urban area. In the LA Basin between March and April, substantial reductions in NO_2 were observed at most measurement sites, but coastal and inland locations had larger decreases in O_3 than the center of the basin (Figs. S1 and S2). In addition to seasonality, meteorological variations at smaller timescales also play an important role in OPE. Examination of the O_3 time-series (Fig. 5) shows a clear correlation between elevated O_3 concentrations and elevated temperature, which was also seen in a preceding analysis of O_3 variations in the

DRAFT

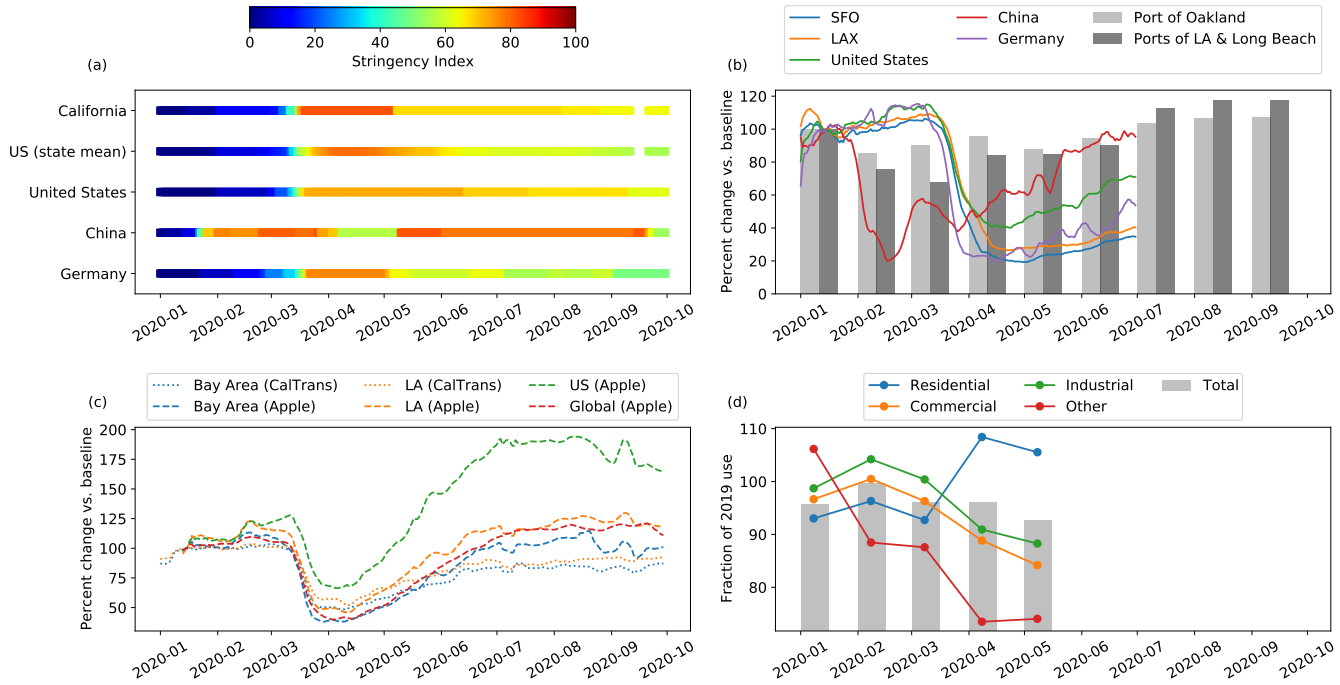

Fig. 3. Metrics for change in human activity at different scales. Panel **(a)** shows the Oxford stringency index (11) for the regions used in this figure. "US (state mean)" is the average of individual states' indices, "United States" is the index attributed to the US as a whole (not individual states). Panel **(b)** shows the percent change in flights(12–14) for two California airports and three countries (lines) and container moves for three California ports (bars) Panel **(c)** shows traffic metrics for two California urban areas, the United States, and 26 countries ("global"). CalTrans indicates Caltrans PEMS data; Apple indicates Apple driving mobility data. Panel **(d)** shows electricity consumption in the US by sector, relative to the same month in 2019. In **(b)** and **(c)**, daily metrics are relative to 15 Jan 2020 and presented as 7 day rolling averages and monthly metrics are relative to Jan 2020. Flight data not available after July 1; electricity consumption not available after May.

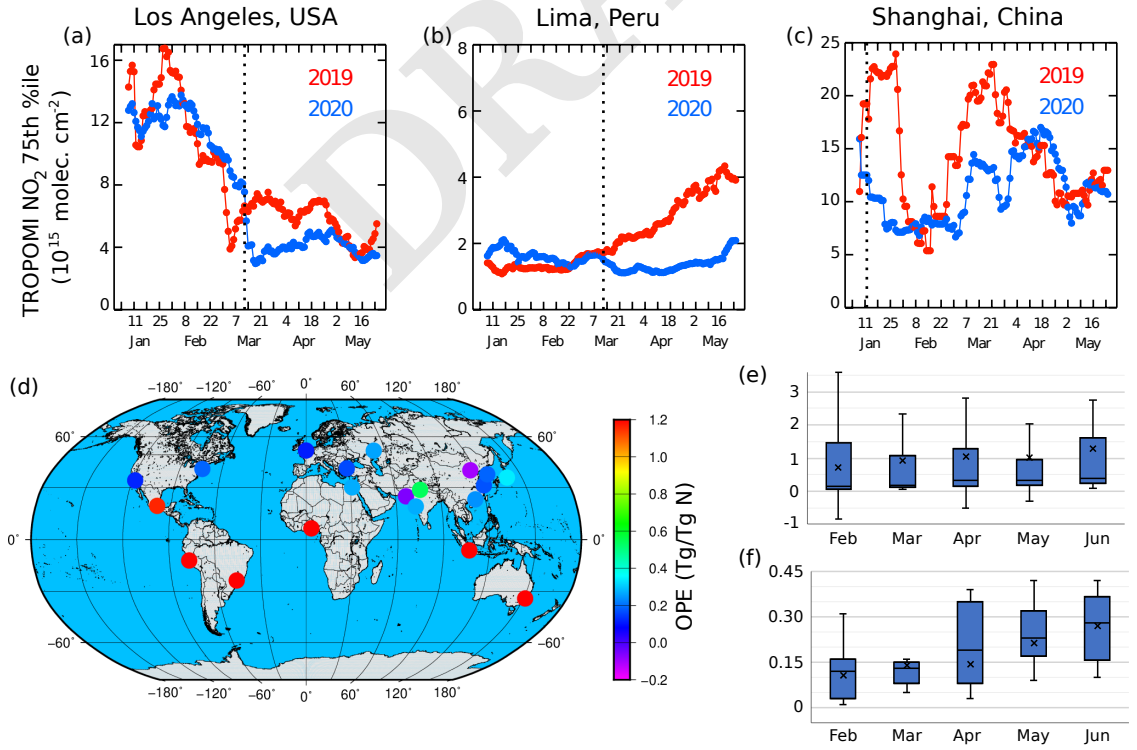

Fig. 4. Changes in NO_2 levels due to COVID-19 lockdowns and resulting change in O_3 production. **(a–c)** 15 day rolling averages of 75th percentile TROPOMI NO_2 column densities in three cities for 2019 and 2020. The vertical dotted line indicates the beginning of lockdown measures in 2020. **(d)** OPE modeled in 17 megacities, averaged from February to June 2020. **(e)** Modeled monthly global averaged tropospheric O_3 production efficiency (OPE). The whiskers are the minimum and maximum, the horizontal lines the quartiles and median, and the X is the mean. **(f)** As in (e), but averaged over 30° N to 90° N.

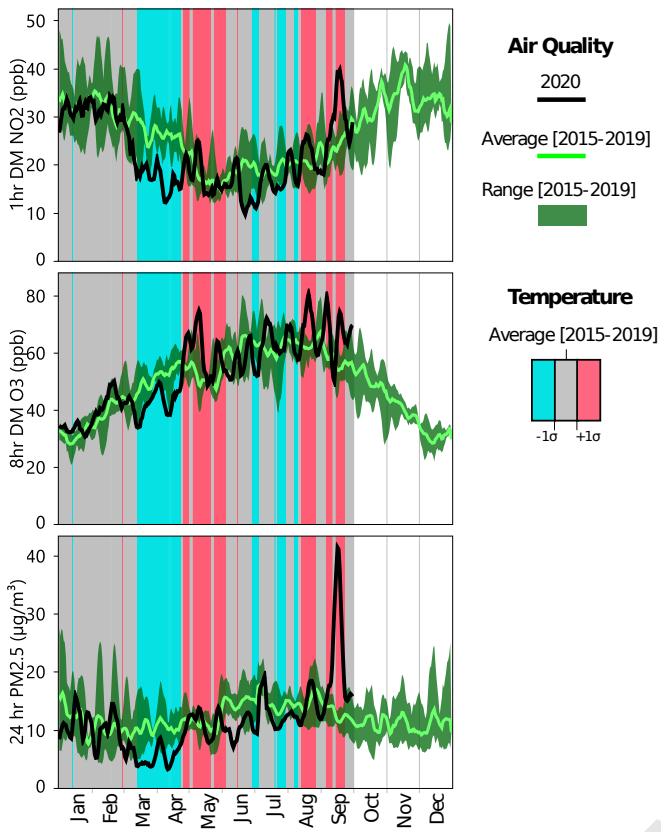

Fig. 5. 7-day rolling average of 24hr $PM_{2.5}$, 1hr daily maximum (DM) NO_2, and 8hr DM O_3 by day of year in 2020 and in the past five years (2015-2019) in the LA Basin. Bars in the background show the 7-day rolling average of basin-average 1 hr DM temperature in 2020 relative to the 2015 to 2019 average ($\pm 1\sigma$) by day of year. 2020 data are preliminary, unvalidated, and subject to change.

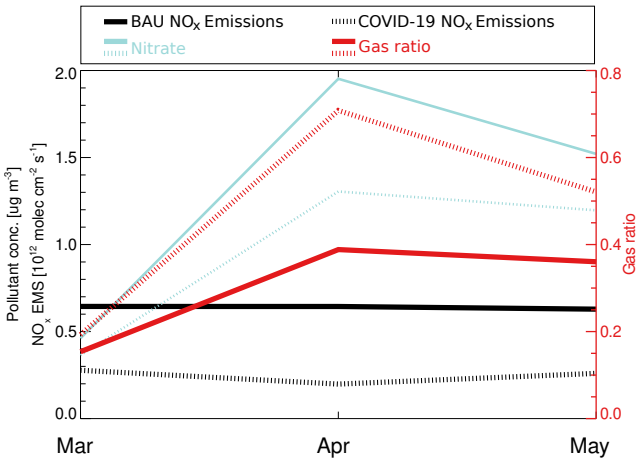

Fig. 6. Simulated inorganic nitrate aerosol sensitivity at downtown LA for two model runs during March to May 2020. Dashed lines represent the run with lockdown-induced emissions reductions (COVID-19), solid lines represent the business as usual (BAU) run. NO_x emissions are shown in black, nitrate aerosol concentration in blue, and the gas ratio in red. A gas ratio < 1 indicates NH_3-limited (compared to NO_x-limited chemistry). See the SI for more information.

LA Basin (21).

The response of particulate pollution to the COVID emissions reductions likewise reveals signatures of both distinct chemical regimes and meteorological controls. $PM_{2.5}$ (particles with diameter ≤ 2.5 μm) levels in the LA Basin were markedly lower than the historical average in March and April (Fig. 5), even before the onset of the COVID-19 lockdown measures in mid-March. Synchronously, the LA Basin experienced frequent stormy days with atypically high amounts of rainfall and increased ventilation of the Basin through higher-than-average wind speeds, likely leading to reduced $PM_{2.5}$ levels through wet deposition and advective removal, respectively. Simulations of inorganic nitrate aerosol formation in the LA Basin under two emissions scenarios, business as usual and COVID-reduced, (Fig. 6) suggest a 20% to 30% decrease in the March to May period due to lower NO_x emissions, with the chemistry shifting substantially towards NO_x-limited under the COVID-reduced emissions scenario. Reduced secondary aerosol formation and a higher degree of wet removal than usual likely both contributed to the reduction in LA Basin $PM_{2.5}$ levels from March to May. After that, $PM_{2.5}$ concentrations reverted to typical levels until mid-September, when massive wildfires significantly deteriorated the air quality in the Basin.

Other measurements, such as carbon monoxide (CO), help to identify the sectors in which emissions were reduced. In urban areas such as Los Angeles, more than 70% of CO emissions are from mobile sources, with smaller contributions from fossil-fueled power plants and other stationary sources (22). As discussed in Section 1, lockdown measures had a very large impact on vehicle miles traveled (VMT) in the LA Basin. This resulted in a clear signal in CO emissions as measured by the CLARS-FTS remote sensing spectrometer on Mt. Wilson (23), overlooking the basin. Figure S4 shows that the CO column abundance decreased by 37.5% in April, 2020 compared with the April mean from 2012-2019. The LA downtown region, where CO concentrations are normally the highest, experienced the largest decrease.

Implications for air quality mitigation strategies. The goal of improving air quality is ultimately to improve human health and quality of life. In this section, we explore what lessons we can learn from the COVID-19 period to inform future air quality policies that rely on cooperative action rather than individual sacrifice. We focus on questions arising from three key results of our analysis. First, what are the implications of the spatial and temporal heterogeneity in the O_3 and $PM_{2.5}$ responses to emissions reductions, at both the global and urban scales? Second, what role does climate play in driving AQ changes, independent of emissions? Third, what lessons from the LA Basin case study can be applied globally, and what are the limitations to doing so?

First, what can be learned from the heterogeneity of the air quality (especially O_3) response to emissions reductions? Globally, the large, relatively constant OPEs of tropical and subtropical megacities suggest that NO_x emissions reductions would be highly effective at reducing O_3 levels throughout the year in these locations, whereas in midlatitudes NO_x decreases primarily impact the summer O_3 season, when OPE values are high relative to the rest of the year. Cities with negative OPE values should consider combined NO_x and VOC controls to minimize short-term increases in O_3 until NO_x concentrations are below the point of peak O_3 production. Urban areas should also assess the potential co-benefits of decreases in nitrate formation associated with NO_x emissions reductions.

DRAFT

The strong dependence of secondary pollutant formation on chemical regime (i.e. the concentration of precursors other than NO_x, including VOCs) as well as the potential for changes in chemical regime induced by simultaneous changes in O_3 and $PM_{2.5}$ concentrations (e.g. increased hydroperoxy radical availability for O_3 production associated with decreased uptake on aerosols (24)) emphasize the need for integrated air quality policies that address multiple types of precursor emissions simultaneously. Finally, the large role of meteorology in controlling air quality (e.g. (18) and Fig. 5) must be taken into account when determining efficient and cost-effective mitigation strategies.

At the urban scale, the variability in observed changes in atmospheric composition within the LA Basin during the COVID-19 lockdowns provides new insights regarding the impacts of air quality policies on environmental justice concerns and human health. COVID-19-related air quality improvements were uneven across population subgroups in the Basin (21) as well as in other major urban areas (15, 25), likely driven by the closer proximity of low-income and minority populations to major emission sources such as large roads, industrial facilities, and ports (26, 27). Observing the health impacts of air quality changes under COVID-19 is complicated because people simultaneously changed the degree to which they sought health care. However, studies have applied concentration-response functions developed under pre-COVID-19 activity patterns to estimate the number of deaths and disease cases that could be avoided if long-term urban planning and environmental policies were to achieve COVID-like levels of emissions reductions (28, 29). The resulting improvements in air quality-related health metrics are substantial, particularly with respect to $PM_{2.5}$, which has an order of magnitude greater impact on premature mortality than O_3 (30). Since air pollution is emerging as a risk factor for COVID-19 severity (31), the COVID-19 experience itself is also highlighting the importance of air pollution mitigation for improving the overall health of populations, making people more resilient to unforeseen risk factors, including novel viruses, in the future.

The second question generated from our analysis is what role does weather and climate play in the observed changes in air quality? Interpreting the changes of O_3 and $PM_{2.5}$ in the LA Basin during COVID-19 is complicated due to colder-than-average temperatures and significant precipitation in March and April and much warmer-than-average temperatures in early May. Separating meteorological effects from responses to emissions reductions must be a key part of follow-on studies of the COVID-19 time period for all locations (15).

The LA Basin measurements, however, represent a unique dataset to compare the relative effects of the O_3 climate penalty (i.e. the increase in O_3 associated with warmer temperatures) against emission reductions. Although not related to the COVID-19 pandemic, multiple prolonged heatwaves in August-October aggravated the O_3 pollution, set records in different parts of the LA Basin, and stretched the O_3 season to early Fall. Similar record-setting heat impacted much of the western US (32). Additionally, intense wildfires throughout California and much of the western US had large impacts on $PM_{2.5}$ levels in the LA Basin. These events demonstrate that climate change and extreme events can undermine air quality progress from emissions controls. A previous prediction of the O_3 climate penalty in 2020 for the LA Basin estimated a basin-average temperature dependence of about 1 ppb K^{-1} and up to 12 ppb K^{-1} in downwind areas (33); however, preliminary analysis suggests typical values of 1.8 to 5.8 ppb K^{-1} for the O_3 season (May-Sep) in 2020 throughout the basin (Fig. S3). Analysis to understand this discrepancy is ongoing. The 2020 wildfire impacts on $PM_{2.5}$ are even greater than those predicted for the end of this century in the first California Climate Assessment (34). Thus, the temperature-dependence of pollutant formation and increases in emissions due to climate change (e.g. temperature-driven evaporative emissions, air conditioning-related electricity generation, chemical production, or extreme wildfire events) mean that climate cannot be considered a separate problem to air quality (35), and policies that target both air quality and climate, such as the recent California executive order requiring all new passenger vehicles sold be zero emission vehicles (36), are critical to the future health of both people and the planet.

Finally, what lessons from the LA Basin case study can be applied globally? Los Angeles has seen decades of emissions controls. In California as a whole, atmospheric levels of CO and VOCs associated with passenger cars were reduced to 2% of their pre-control levels by 2010 (37) and the entire diesel truck fleet was converted to lower NO_x and $PM_{2.5}$ technologies by 2020 (38). Passenger cars and light trucks now represent only about 10% of total NO_x emissions in the LA Basin, while heavy-duty trucks and buses represent approximately 30% (39). Thus it is not completely unexpected that the O_3 and $PM_{2.5}$ impacts of the COVID-19 reduction in traffic in LA, the majority of which was associated with passenger vehicles, are small compared to meteorological influences. Due to the continuing success of emissions controls on transportation sources, other sources of NO_x (e.g., off-road diesel sources), VOCs (volatile chemical products), and background O_3 are becoming relatively more important to the O_3 budget in LA (19, 40). Cities that still have a large fraction of emissions coming from passenger vehicles should not expect meteorological effects to overwhelm efforts to reduce pollutant formation from vehicular emissions; rather, meteorology will set the lower bound of O_3 and $PM_{2.5}$ concentrations attainable solely through emissions controls.

We note that the maximum COVID-19 disruptions in California were during spring, when both O_3 and $PM_{2.5}$ are typically at their minimum levels and well below the U.S. ambient air quality standards. However, late-April and early-May O_3 levels were higher than in recent years in the LA Basin, which raises the question of whether there might be a shift in the seasonality of O_3 concentrations in the future (40). More work is needed to fully disentangle the effects of emissions, meteorology, and climate change in this regard.

While most of the policy implications described here are neither particularly new nor surprising, the COVID-19 event, combined with extensive ground- and satellite-based observations, has allowed us to confirm our expectations of the impacts of NO_x emissions reductions on air quality and atmospheric composition to a degree never before possible. To summarize, the major lessons learned are:

1. Atmospheric chemistry and other processes alter the efficacy of emissions controls from month to month, city to city, and even neighborhood to neighborhood.

2. Care must be taken when crafting mitigation policies

DRAFT

to ensure disadvantaged neighborhoods benefit equally under new policies and that any pre-existing disparities are addressed.

3. In a warmer future climate with strong limits on AQ emissions, climate-driven AQ responses can overwhelm local controls. Therefore, controls on GHGs should be included in air quality mitigation strategies.

4. When applying our results from the LA Basin to other locations, it is important to note that (a) passenger vehicles and light trucks now represent only about 10% of LA NO_x emissions and (b) the peak COVID-19 emissions reduction occurred outside of the typical O_3 season (May-Sep). Additional work is required to fully understand how this result transfers to the summer months and to cities with a higher proportion of emissions from passenger vehicles. Nevertheless, points 2 and 3 are still generally applicable.

3. Observed changes in GHGs and implications for mitigation strategies

GHG Observations. As with air quality, lockdowns associated with the COVID-19 pandemic illustrate the link between individual activity and fossil fuel GHG emissions. However, surface transportation, where most of the reductions occurred, comprises only 21% of global CO_2 emissions, while power generation accounts for 44% (1). Thus, the large local changes in individual mobility, which represent a significant disruption to everyday life, had a limited global impact, with emissions going back in time only about a decade (Fig. 2a). Furthermore, unlike air quality, which responds quickly to changes in source gases, the effect of emissions perturbations on atmospheric CO_2 concentrations is buffered by its much longer effective lifetime. Observing the impact of COVID-19 on atmospheric CO_2 at global-to-regional scales has therefore proven difficult. However, in urban areas with CO_2 monitoring networks such as the San Francisco Bay Area, changes in both emissions and atmospheric concentrations were much larger; observations from the Bay Area are discussed in detail below.

Our preliminary estimates suggest that the global reduction in anthropogenic CO_2 emissions was 7.8% for Jan-August 2020 relative to 2019 (2) (Fig. 7a). Reductions were greatest in April, recovering to just below 2019 levels by mid-August. The year-average decline of the global emission could be 5% to 10% (approx. 490 to 980 Tg C) depending on the intensity of the reduction during the remaining lockdowns and the timing of the return of economic activity to pre-pandemic levels.

The impact on atmospheric concentrations, however, was much smaller. Because the CO_2 lifetime is long in the Earth system, present-day concentrations reflect accumulated emissions over decades to centuries, as well as positive and negative feedbacks. The atmospheric CO_2 mixing ratio has increased dramatically in the past decades. Current levels exceed 400 ppm, having increased every year without fail since the modern record began in 1958, when CO_2 was just over 300 ppm. In addition, there is a clear seasonal cycle, driven by the terrestrial biosphere, as well as natural interannual variability due to climate (e.g. tropical drought (41, 42)) and changes in atmospheric circulation patterns. Natural variability in terrestrial and ocean fluxes, which respond to concentration changes as well as to climate and human land use, can compensate for or magnify anthropogenic emissions changes. This reduces the detectability of a global signal of even quite large regional emission changes.

Figure 7b shows both the observed mixing ratios at the Mauna Loa observatory and simulated mixing ratios using the Goddard Earth Observing System (GEOS) atmospheric model that incorporates daily estimates of 2019 and 2020 emissions from Liu et al. (2) This analysis shows that the impact of COVID-19 emissions reductions on the total mixing ratio in the atmosphere is quite small and hard to detect against the background seasonality and the long-term increasing trend. During early April, the time period with the sharpest emissions decreases associated with COVID-19, the impact on CO_2 at Mauna Loa was only a fraction of a ppm, which is smaller than interannual climate-driven changes caused by the El Niño cycle (41). For context, over the past 5 years, CO_2 at Mauna Loa has increased by nearly 15 ppm.

Ocean and land biosphere feedbacks may play a crucial role in reducing the atmospheric signal of CO_2 emissions reductions. One hypothesis is that carbon uptake by the ocean will decrease with smaller carbon emissions. This hypothesis is supported by the ensemble of model simulations shown in Figure 8, which depicts the responses of ocean and terrestrial carbon fluxes under both a typical emissions scenario and COVID-19-like emissions (43). Although the land flux is similar in both scenarios, ocean uptake decreases in response to the reduced atmospheric CO_2 growth rate (44). We find that the ocean uptake reduction of approximately 70 TgC/yr for 2020 offsets 7% to 14% of the reduction in anthropogenic emissions.

In contrast with the minimal changes in the trajectory of CO_2 globally, much larger changes have been observed locally. Turner et al. (45) compared 6 weeks of CO_2 measurements before and after mobility restrictions were enacted in the San Francisco Bay Area and observed a 5-50 ppm decrease; from this, they inferred a 30% decrease in fossil fuel CO_2 emissions over the period (Fig. 7c). When integrated over the first six months of the year, COVID-19 restrictions represent an almost 80% total reduction in CO_2 emissions from vehicles in the Bay Area relative to 2019. The decrease in mobility also perturbed the daily and weekly cycle of emissions, with the largest reductions occurring mid-week and during the morning rush hour. The atmospheric CO_2 signal was observable in an urban area because of the proximity to the perturbed sources, in contrast to the dilute, global signal.

The nature of the Bay Area human system means that traffic emissions are a significant driver of near-field CO_2 mixing ratios. Other large urban areas also experienced significant declines in emissions from ground transportation, with approximately 70% reductions in New York and Beijing when the lockdowns started (46). At the regional scale, other emission sectors had more influence. Gurney et al. (47, 48) found that weekly total US fossil fuel CO_2 emission reached a maximum departure of -19.5% (-18.2% to -21.6%) during the week ending April 3, 2020, consistent with the initiation of state-scale COVID-19 lockdown orders. The average fossil fuel CO_2 emissions decline for April and May, the two-month period with the largest persistent reduction, was -15.8% (-14.3% to -17.8%), with the largest decrease from gasoline-fueled transportation (-30.2%), followed by electricity generation (-15.4%), aviation (-62.2%), and industrial activity (-9.0%). Hence, while mobility sectors did have the largest decrease across the US, other

DRAFT

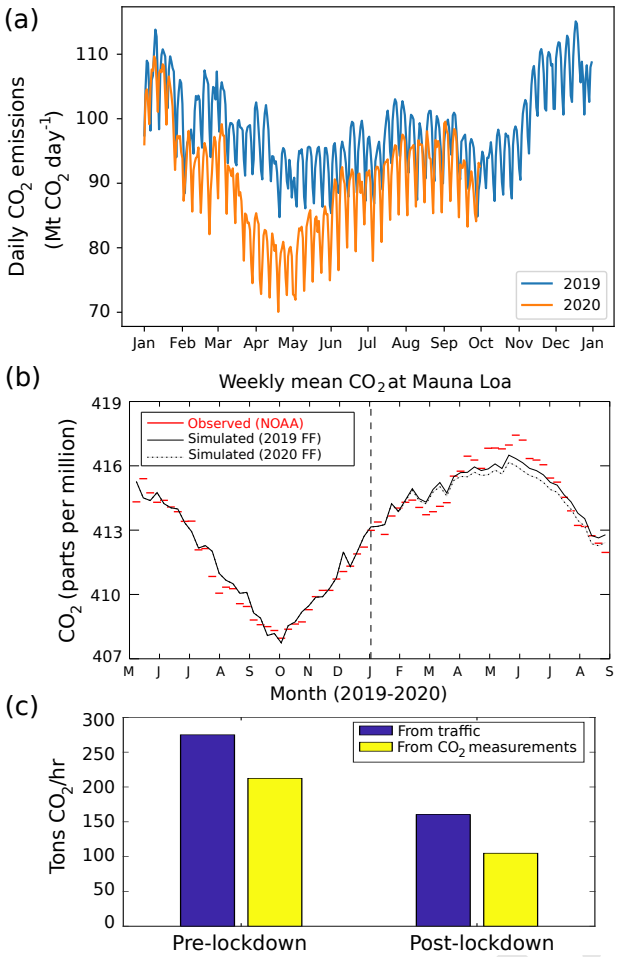

Fig. 7. (a) Global CO_2 emissions for 2019 and 2020. See SI for details. **(b)** Simulated (black) and weekly average observed (red) CO_2 at the Mauna Loa observatory (49) during 2019 and 2020. A GEOS simulation assuming 2019 emissions levels in 2020 is shown as the solid black line along with a simulation incorporating estimated 2020 decreases (dashed black line). **(c)** CO_2 emissions in the San Francisco Bay Area before and after the COVID-19 lockdown, inferred through two techniques: an inversion of $BEACO_2N$ network observations ("from CO_2 measurements") and traffic data combined with estimates of fuel efficiency ('from traffic").

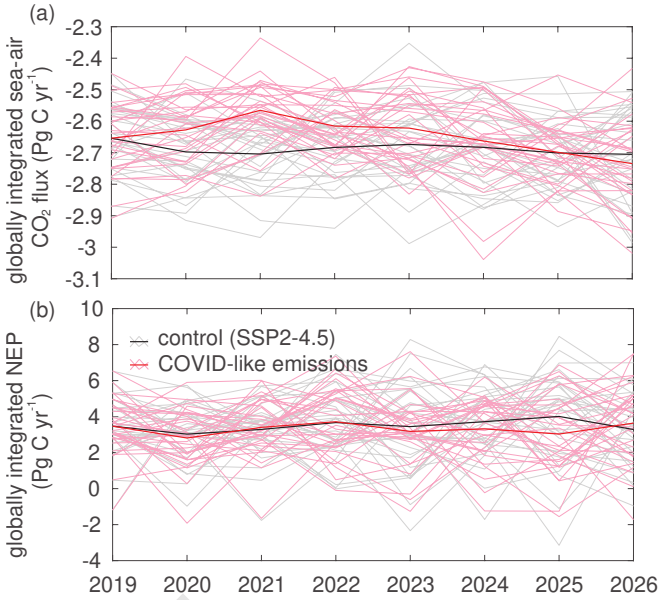

Fig. 8. Annual mean, globally integrated carbon dioxide fluxes predicted from the CanESM5-COVID ensemble (43): **(a)** Sea-to-air CO_2 flux (positive out of ocean; Pg C yr^{-1}), and **(b)** terrestrial net ecosystem production (NEP, positive into biosphere, excludes land use change, Pg C yr^{-1}). Black/gray lines derive from simulations forced with SSP2-RCP4.5 CO_2 emissions, while red/pink lines derive from simulations forced with a 25% peak CO_2 emissions reduction in 2020. See (43) for more details. Thick lines are ensemble averages, and thin lines are individual ensemble members, each with different phasing of internal variability.

sectors also experienced anomalous declines. When including expectations for the remainder of 2020, the estimated annual fossil fuel CO_2 emissions decline in the U.S. is projected to be -9.9% (-7.6% to -12.1%). These differences in local, regional, and global changes in emissions and atmospheric concentrations of CO_2 emphasize the need for monitoring CO_2 at multiple scales.

While there is a clear chain of causality tying COVID-19 mobility restrictions to CO_2 emissions, the impacts of COVID-19 on other major GHGs such as methane are less clear. The fossil fuel sector is indeed a major source of methane; however, methane emissions are not directly tied to fossil fuel combustion. Instead, they occur during the production, processing, and transport of oil and gas as well as from coal mining. The COVID-19 lockdowns imply a number of competing effects with respect to methane emissions. Oil production declined, but the demand for methane for heating and power generation may not have changed significantly. Drilling of new wells decreased; at the same time, production and storage facilities may have reduced the maintenance frequency, leading to an increase in leaks. In response to these uncertainties, NASA organized an airborne campaign in the spring of 2020 to better understand the processes controlling methane emissions during COVID-19. The campaign aimed to leverage the recent work of Duren *et al.* (50) who used an airborne imaging spectrometer (51) to characterize methane emissions across California. Analysis of these results is ongoing.

In addition to direct changes in methane emissions, the growth rate of CH_4 in the atmosphere will be impacted by the shift in NO_x chemistry seen in Sect. 2. In a model incorporating the decreased NO_x emissions associated with COVID-19 (20), March to June monthly global averaged OH concentrations decreased by 2% to 4%. Using the tropospheric chemical methane lifetime from the Atmospheric Chemistry Climate Model Intercomparison Project (ACCMIP) multi-model mean (9.3 ± 1.6 year), a 4% OH reduction would increase the methane lifetime by about 4 months, roughly equivalent to a 22 Tg/yr (6%) increase in fossil fuel methane emissions (Fig. 2).

Implications for GHG mitigation strategies. Though the effect of COVID-19-induced lockdowns on the growth rate of atmospheric CO_2 was small, this event provided important information on how the Earth system and human behavior respond to a sudden shift in emissions, and demonstrates that restriction of personal mobility is not an effective means of reducing atmospheric CO_2. For methane, any decreases in emissions can be counteracted by NO_x reductions and the resulting increases in lifetime, indicating once again the importance of designing integrated climate and AQ mitigation policies.

The San Francisco Bay Area provides an example of how

DRAFT

behavioral responses to the pandemic can offset potential emissions reductions. VMT in the Bay Area decreased in the first six weeks after safer-at-home measures were imposed, followed by recovery in the late spring and summer months. As of June 2020, VMT has largely recovered, reaching 83% of the baseline despite 40% of people in the Bay Area still reporting staying at home. One reason for the recent increases in VMT may be a combination of a reluctance to use and a reduction of services in public transit. Monthly ridership of the Bay Area Rapid Transit System (BART) saw an average of roughly 400,000 riders daily on pre-pandemic weekdays. Ridership reductions relative to February 2020 peaked in April, with a 93% decrease in BART usage. In contrast to personal vehicle use, BART ridership has recovered only slightly in recent months, with ridership in September still 87% below February levels (https://www.bart.gov/about/reports/ridership, last accessed 29 Oct 2020).

At the same time, COVID-19 has the potential to lead to local permanent emissions reductions. The Marathon Refinery, which represents roughly 10% of Bay Area industrial CO_2 emissions (52), ceased operations permanently in 2020 and is under evaluation for use as a renewable diesel processing facility (https://www.sfchronicle.com/business/article/Marathon-Petroleum-will-indefinitely-idle-15451841.php, last accessed 29 Oct 2020).

Complex recovery paths further complicate understanding the long-term effects of COVID-19 on CO_2 (and CH_4), but they also provide insights into the challenges of observing and verifying more intentional mitigation of emissions in the complex carbon energy system as the world addresses climate change. There are two key conclusions to draw from this analysis:

1. Changes in both human behavior and the Earth system can counteract reductions in GHG emissions. While there were examples of positive feedbacks (e.g. the Marathon refinery closure), the net impact appears to be a partial offset of the emissions reductions. In particular, oceanic uptake of CO_2 rapidly decreased, which immediately offset part of the anthropogenic emissions reduction. Therefore, we must expect that the ratio between the change in the atmospheric growth rate of GHGs and changes in emissions is less than one, and plan accordingly.

2. Despite the major disruption that the COVID-19 pandemic has caused in most people's lives, it has had little effect on the trajectory of our future climate. The contrast between stark emissions reductions across the transportation sector and the minimal impact on global CO_2 concentrations highlights the ineffectiveness of piecemeal or single-sector emissions reductions at slowing global accumulation of GHGs. This paradox demonstrates the dire need for systemic change, rather than extreme modification of individual behavior, to effectively mitigate climate change. GHG emissions from all of the largest sectors: power generation, industry, transportation, and agriculture (1, 53) must be addressed to permanently move our CO_2 and CH_4 emissions back in time and effectively reduce their concentrations in the atmosphere.

4. Earth observing system: successes and future vision

Understanding the global atmospheric response to COVID-19 mitigation policies would not have been possible without international investments in both ground-based and space-based environmental sensors (54, 55). In the sections above, we have shown that the current observing system, combined with data assimilation and modeling frameworks that allow us to tease apart the roles of COVID-induced emissions reductions, meteorology, and biospheric processes, is able to deliver an understanding of the processes mediating the production, transport, and removal of air pollutants and GHGs. At the same time, this analysis of COVID-19 impacts on the atmosphere has revealed gaps in the observing system.

Quantifying the emissions, transport, and transformation of atmospheric pollutants is a multi-scale challenge in both space and time. An effective observing system must capture the non-linearity in chemistry associated with changes in emissions on urban scales and the subsequent impact of these changes on regional and global scales. A specific gap in AQ observing capability is high-quality, routine measurements of volatile organic compounds. For GHGs, the global observing system must simultaneously be able to break down the sector-by-sector contribution to GHG emissions and detect the Earth system responses to these emissions changes. These goals require additional observations and measurements at finer spatial and temporal resolution than currently available.

The current fleet of GHG observing satellites is limited to narrow field-of-view instruments in low earth orbit, meaning a given location is only observed once per day and the number of locations observed is limited. While current air quality observing satellites include wide swath instruments capable of global coverage, they have still been restricted to at most twice daily observations up until now. Over the next decade, however, a new suite of geostationary sounders will provide air quality data at unprecedented spatio-temporal resolutions as part of a global air quality constellation (56). The first of these sounders, the Geostationary Environment Monitoring Spectrometer (GEMS), launched recently and will provide hourly air quality measurements over Asia. The diurnally resolved measurements should provide information to help distinguish between various emissions sectors. GEMS will soon be followed by TEMPO over North America (57) and Sentinel-4 over Europe and North Africa (58). Similar plans are in motion to launch next generation GHG observing satellites, including geoCARB (59), GOSAT-GW (60), and CO2M (61) which will provide much denser CO_2 observations than the current fleet of CO_2 sensors. Other proposed missions, such as the Atmospheric Imaging Mission for Northern Regions (62), would bring a dense set of air quality and GHG observations to the northern high latitudes, critical for understanding how the boreal forest and permafrost respond to climate change.

The observing system of the future also needs to be able to resolve lower atmospheric variability and extend the number of species observed. The LA Basin AQ example showed the importance of understanding the chemical regime that governs O_3 and $PM_{2.5}$ formation, and of other tracer measurements such as CO to disambiguate different sectors' emissions. New approaches will combine measurements from multiple sensors to infer near-surface quantities relevant to AQ (63, 64). Augmenting the planned next generation of satellites, which cover

DRAFT

the short wave infrared, near infrared, visible, and ultraviolet wavelengths, with thermal infrared sensors will aid in this. This could be feasible from meteorological sounders like IRS-MTG (65), though higher spectral resolution than currently planned for meteorological sounders is critical for quantifying near-surface O_3. Retrievals of isoprene, the largest natural VOC source, have recently been demonstrated using thermal IR measurements from the Cross-track Infrared Sounder (CrIS) (63). Designing an isoprene-specific instrument with a lower limit of detectability than CrIS and concurrently measuring HCHO and NO_2 would provide key information on chemical regimes relevant to O_3 and secondary aerosol formation.

Measurements of particulates, which according to the Global Burden of Disease are the leading environmental risk factor for mortality, have unique challenges relative to those of trace gases. Although advances in the retrieval of AOD from satellite measurements of solar backscatter (66, 67), coupled with observed relationships between AOD and $PM_{2.5}$, are offering a new window into air quality assessment from satellite remote sensing (68, 69), challenges remain in observing how emissions changes such as those associated with COVID-19 interventions interact with the $PM_{2.5}$ chemical system. Given the dichotomy in the response to COVID-19 emissions reductions seen between urban and rural areas (Figs. S5–S7), working towards $PM_{2.5}$ observations that cover both types of regions, either through wider in situ networks, new developments in remote sensing (70, 71), or a combination of both (72, 73), will be important to understand the chemical factors controlling $PM_{2.5}$ exposure.

Though the ability of satellite measurements to provide global coverage is invaluable for monitoring global air quality and GHG burdens, a space-based system must be complemented with innovative in situ approaches. These approaches provide important information on the vertical distribution of atmospheric constituents (74) at small spatiotemporal scales to complement space-based column abundances, as well as measurements of critical species that cannot be measured by remote sensing techniques.

Dense, low cost sensor networks such as the Berkeley $BEACO_2N$ network (75, 76) can play an important role in resolving urban-scale pollution. These networks effectively offer a mapping capability similar to the next generation of space-based observations, but through a distributed collection of instruments, rather than a single imager. Section 3 described how $BEACO_2N$ measurements informed estimates of CO_2 emissions reductions due to COVID in the San Francisco Bay Area. Other networks that have likewise observed high spatial variability in CO_2 and pollutant gases as well as temporal variations caused by local emissions have been reported in Pittsburgh, PA, USA (77, 78), and Cambridge, UK (79, 80).

Sensor networks can be especially useful in distinguishing between emissions from different sectors. Low cost sensors deployed at Heathrow Airport in the UK were used to refine a NO_x emission inventory by constraining the emission ratio between NO_x and CO_2 (81). Another study in Pittsburgh, PA (82) that focused on the impact of COVID-19 found a 50% reduction in CO and NO_2, leading to a 100% reduction in the typical $PM_{2.5}$ enhancement from traffic during morning rush hours, but no significant change in industry-related CO and $PM_{2.5}$ concentrations. These studies highlight a particular advantage of in situ networks over space-based observations: not only do they offer higher temporal resolution than even geostationary sensors, but they can measure at night and early morning, when sunlight-observing spectrometers cannot. Finding ways to integrate measurements from in situ networks and Earth observing satellites will enable us to combine the best aspects of both. One study (73) did so successfully and reported greater accuracy and spatiotemporal detail in $PM_{2.5}$ exposure estimates.

In between these neighborhood-level networks and orbiting satellites, a system must include a component capable of deploying in a rapid response mode to measure quickly-evolving changes in the Earth system. Section 3, showed how the response of the CH_4 growth rate to the COVID-19 pandemic is governed by both changes in emissions and lifetime. At the global scale, these will be convolved and very challenging to separate. The NASA aircraft campaign organized to study methane emission processes during spring of 2020 will provide critical, near-field data (unaffected by changes in lifetime) to separate these factors. Such targeted observations that can be deployed as needed must be part of future observing system plans.

Given the focus on dense monitoring networks and high spatiotemporal frequency satellite observations, it is clear that the volume of data available will continue to grow in the future. Data-driven modeling is a key tool to separate out the various processes at work in the Earth system. Therefore the development of infrastructure for synthesis of these datastreams must accompany the deployment of new satellite constellations and in situ networks. Another requirement is the development of models that can seamlessly represent the chemical environment from urban to global scales. The MUlti-Scale Infrastructure for Chemistry and Aerosols (MUSICA) (83), is an example of the initial development of such a framework. Data assimilation, which is the cornerstone of modern numerical weather prediction, is a critical pillar for the global analysis of air quality constrained by observations and for CO_2 flux estimate efforts. New initiatives like the European Copernicus Atmospheric Modeling Service (CAMS) (84) are providing an operational capacity for air quality while new systems are focused on estimating both emissions and pollutants (20, 85). Additional data assimilation tools are needed that can integrate the growing datastreams and capture (1) the evolving nonlinear relationships between the large suite of chemical constituents, (2) the broad range of chemical lifetimes and spatial scales involved, and (3) the offsetting responses occurring in the Earth system. The development of these tools as a community-based resource should be a component of the emerging observing system to ensure that the broader community can effectively exploit the observations to better understand the changing Earth system.

Conclusion

The COVID-19 pandemic represents an unprecedented and well-observed event that provides a glimpse into both the past and a future world with drastically altered emissions to the atmosphere. Much work remains to be done to understand in detail the implications of this event for understanding human interaction with the Earth system. However, the availability of an unprecedented wealth of Earth observations during the pandemic shows the value of current and future space-based

DRAFT

and in situ sensors in understanding these interactions. Several key lessons are already apparent from these systems and the nascent integrated analyses presented here.

The chemical regimes governing the response of air quality to emissions changes are quite variable in both space and time. Future actions to remediate air quality should consider the best course for a given location, and be careful about applying lessons from historically successful actions without accounting for differences between then and now. Even within a single city, spatial differences in the air quality response to emissions must be considered to ensure all neighborhoods benefit from air quality improvements.

Despite the massive disruption to daily life around the world, the lockdowns resulting from the COVID-19 pandemic brought our CO_2 emissions back in time by only nine years. Coupled with changes in ocean flux and human behavior that partly offset the reduction, the pandemic did not significantly reduce the growth rate of atmospheric CO_2. Clearly, changes in individual behavior alone will not prevent our reaching a 1.5°C warming. Sustained, systemic changes are required to curb our carbon emissions.

Observations during the COVID-19 period show unambiguously that improving air quality and preventing climate change are not separate problems; they are inextricably linked. Climate-driven extremes of temperature, drought, and wildfires can overwhelm a half century of effort to improve air quality. Simultaneously, reduced NO_x emissions can lead to longer CH_4 lifetime through reduced OH concentrations, increasing methane's warming potential. As depicted in Fig. 1, strategies to achieve better air quality and reduce climate change can be informed by the results presented here and depend on solutions that treat these as two parts of the same goal, and not separate challenges.

Materials and Methods

Full methods are available in the SI. Analysis of LA Basin air quality used data from CA Air Resources Board monitors, filtered for complete data records in the 2015 to 2020 period. Model simulations to derive OPE used multiconstituent assimilation in the MIROC-CHASER model. OPE calculated by comparing modeled O_3 production difference between baseline and reduced 2020 emissions. $PM_{2.5}$ simulations used GEOS-Chem v9-02 with NO_x emissions consistent with the OPE simulations.

SF Bay Area CO_2 emissions were estimated by (a) an inversion of $BEACO_2N$ network CO_2 measurements using the STILT model (86) and (b) by the product of PeMS-measured VMT and fleet fuel efficiency. Global CO_2 emissions estimates were derived from an array of near-real time data on power generation, industry, transport, and fuel consumption.

Publicly available datasets will be listed in the SI. For other datasets, please contact the corresponding authors.

ACKNOWLEDGMENTS. The authors thank the Keck Institute for Space Studies for organizing and supporting the study "COVID-19: Identifying Unique Opportunities for Earth System Science" that led to the writing of this manuscript. The authors also acknowledge the use of data from the Port of Oakland and Port of LA website, Apple mobility data, and US EIA electricity use data. The authors also thank Charles Carter for his artwork in Figure 1. The views expressed in this manuscript are solely those of the authors and do not necessarily reflect those of the South Coast Air Quality Management District. A portion of this research was carried out at the Jet Propulsion Laboratory, California Institute of Technology, under contract with NASA. The authors acknowledge funding from the NASA and NSF: NASA grant NNX17AE15G (JL and PW), NASA CMS grant 80NSSC20K0006 (AC), NASA grant 80NSSC18K0689 (DH and HC), NASA Aura Science Team Program 19-AURAST19-0044 (KM and K. Bowman), NASA grant 80NSSC20K1122 (DG and SA), NSF RAPID grant 2030049 (K. Barsanti), NSF grants OCE-1752724 and OCE-1948664 (NL), and NSF grant OCE-1948624 (GM). AJT was supported as a Miller Fellow with the Miller Institute for Basic Research in Science at UC Berkeley. KG was supported by Northern Arizona University startup funds. CI was supported by University of California Institute of Transportation Studies. SS and ZZ were supported by California Air Resources Board, NASA Science Mission Directorate/Earth Science Division and JPL Earth Science and Technology Directorate. YLY was supported in part by the Jet Propulsion Laboratory OCO-2 grant JPL.1613918 to Caltech.

1. C Le Quéré, et al., Temporary reduction in daily global CO_2 emissions during the COVID-19 forced confinement. *Nat. Clim. Chang.* **10**, 647–653 (2020).
2. Z Liu, et al., COVID-19 causes record decline in global CO_2 emissions (2020) arXiv:2004.13614.
3. K Miyazaki, et al., Decadal changes in global surface NO_x emissions from multi-constituent satellite data assimilation. *Atmospheric Chem. Phys.* **17**, 807–837 (2017).
4. Z Jiang, et al., Unexpected slowdown of US pollutant emission reduction in the past decade. *Proc. Natl. Acad. Sci.* **115**, 5099–5104 (2018).
5. NA Krotkov, et al., Aura OMI observations of regional SO_2 and NO_2 pollution changes from 2005 to 2015. *Atmospheric Chem. Phys.* **16**, 4605–4629 (2016).
6. B Hassler, et al., Analysis of long-term observations of NO_x and CO in megacities and application to constraining emissions inventories. *Geophys. Res. Lett.* **43**, 9920–9930 (2016).
7. Z Qu, DK Henze, OR Cooper, JL Neu, Impacts of global NO_x inversions on NO_2 and ozone simulations. *Atmospheric Chem. Phys.* **20**, 13109–13130 (2020).
8. JE Jonson, D Simpson, H Fagerli, S Solberg, Can we explain the trends in European ozone levels? *Atmospheric Chem. Phys.* **6**, 51–66 (2006).
9. European Monitoring and Evaluation Programme (2020) https://www.emep.int/index.html, last accessed 10 Nov 2020.
10. RJ van der A, et al., Cleaning up the air: effectiveness of air quality policy for SO_2 and NO_x emissions in China. *Atmospheric Chem. Phys.* **17**, 1775–1789 (2017).
11. T Hale, et al., Oxford COVID-19 government response tracker. Blavatnik School of Government. (2020).
12. M Strohmeier, X Olive, J Lübbe, M Schäfer, V Lenders, Crowdsourced air traffic data from the OpenSky network 2019–20. *Earth Syst. Sci. Data Discuss.* **2020**, 1–15 (2020).
13. M Schäfer, M Strohmeier, V Lenders, I Martinovic, M Wilhelm, Bringing Up OpenSky: A Large-scale ADS-B Sensor Network for Research. *Proceedings of the 13th IEEE/ACM International Symposium on Information Processing in Sensor Networks (IPSN)*, 83–94 (2014).
14. X Olive, traffic, a toolbox for processing and analysing air traffic data. *J. Open Source Softw.* **4** (2019).
15. DL Goldberg, et al., Disentangling the impact of the COVID-19 lockdowns on urban NO_2 from natural variability. *Geophys. Res. Lett.* **47** (2020).
16. J Ding, et al., NO_x emissions reduction and rebound in China due to the COVID-19 crisis. *Geophys. Res. Lett.* **47**, e2020GL089912 (2020) e2020GL089912 2020GL089912.
17. H Simon, A Reff, B Wells, J Xing, N Frank, Ozone trends across the United States over a period of decreasing NO_x and VOC emissions. *Environ. Sci. & Technol.* **49**, 186–195 (2015) PMID: 25517137.
18. T Le, et al., Unexpected air pollution with marked emission reductions during the COVID-19 outbreak in China. *Science* **369**, 702–706 (2020).
19. BC McDonald, et al., Volatile chemical products emerging as largest petrochemical source of urban organic emissions. *Science* **359**, 760–764 (2018).
20. K Miyazaki, et al., Updated tropospheric chemistry reanalysis and emission estimates, TCR-2, for 2005–2018. *Earth Syst. Sci. Data* **12**, 2223–2259 (2020).
21. C Ivey, et al., Impacts of the 2020 COVID-19 Shutdown Measures on Ozone Production in the Los Angeles Basin, preprint (2020).
22. ZC Zeng, et al., Tracking the atmospheric pulse of a North American megacity from a mountaintop remote sensing observatory. *Remote. Sens. Environ.* **248**, 112000 (2020).
23. KW Wong, et al., Mapping $CH_4 : CO_2$ ratios in Los Angeles with CLARS-FTS from Mount Wilson, California. *Atmospheric Chem. Phys.* **15**, 241–252 (2015).
24. K Li, et al., Anthropogenic drivers of 2013–2017 trends in summer surface ozone in China. *Proc. Natl. Acad. Sci.* **116**, 422–427 (2019).
25. G Kerr, D Goldberg, S Anenberg, COVID-19 lockdowns reveal pronounced disparities in nitrogen dioxide levels. (in prep.).
26. HJ Lee, HY Park, Prioritizing the control of emission sources to mitigate PM2.5 disparity in California. *Atmospheric Environ.* **224**, 117316 (2020).
27. SS Park, A Vijayan, SL Mara, JD Herner, Investigating the real-world emission characteristics of light-duty gasoline vehicles and their relationship to local socioeconomic conditions in three communities in Los Angeles, California. *J. Air & Waste Manag. Assoc.* **66**, 1031–1044 (2016).
28. J Chen, et al., Methane emissions from the Munich Oktoberfest. *Atmospheric Chem. Phys.* **20**, 3683–3696 (2020).
29. K Miyazaki, et al., Air quality response in China linked to the 2019 novel coronavirus (COVID-19) lockdown. *Geophys. Res. Lett.* **47**, e2020GL089252 (2020) e2020GL089252 10.1029/2020GL089252.
30. Q Di, et al., Air pollution and mortality in the medicare population. *New Engl. J. Medicine* **376**, 2513–2522 (2017).
31. X Wu, RC Nethery, MB Sabath, D Braun, F Dominici, Air pollution and COVID-19 mortality in the United States: Strengths and limitations of an ecological regression analysis. *Sci. Adv.* **6** (2020).
32. NOAA, (2020) https://www.ncdc.noaa.gov/temp-and-precip/us-maps/1/202008?products[]=countytavgrank#maps, last accessed 23 Nov 2020.

DRAFT

33. DJ Rasmussen, J Hu, A Mahmud, MJ Kleeman, The ozone–climate penalty: Past, present, and future. *Environ. Sci. & Technol.* **47**, 14258–14266 (2013).
34. DR Cayan, et al., Overview of the California climate change scenarios project. *Clim. Chang.* **87**, 1–6 (2008).
35. PB Duffy, et al., Strengthened scientific support for the endangerment finding for atmospheric greenhouse gases. *Science* **363**, eaat5982 (2018).
36. Office of Governor Gavin Newsom, Fossil fuel in California's fight against climate change (2020) https://www.gov.ca.gov/2020/09/23/governor-newsom-announces-california-will-phase-out-gasoline-powered-cars-drastically-reduce-demand-for-fossil-fuel-in-californias-fight-against-climate-change/, accessed 10 Nov 2020.
37. C Warneke, et al., Multiyear trends in volatile organic compounds in Los Angeles, California: Five decades of decreasing emissions. *J. Geophys. Res. Atmospheres* **117** (2012).
38. KH Kozawa, SS Park, SL Mara, JD Herner, Verifying emission reductions from heavy-duty diesel trucks operating on southern California freeways. *Environ. Sci. & Technol.* **48**, 1475–1483 (2014).
39. CAR Board, CEPAM standard emission tool, annual-average NO_x emissions in the South Coast Air Basin for 2020. (year?) https://ww2.arb.ca.gov/emission-inventory-data, accessed November 2, 2020.
40. DD Parrish, LM Young, MH Newman, KC Aikin, TB Ryerson, Ozone design values in southern California's air basins: Temporal evolution and U.S. background contribution. *J. Geophys. Res. Atmospheres* **122**, 11,166–11,182 (2017).
41. J Liu, et al., Contrasting carbon cycle responses of the tropical continents to the 2015–2016 El Niño. *Science* **358** (2017).
42. B Poulter, et al., Contribution of semi-arid ecosystems to interannual variability of the global carbon cycle. *Nature* **509**, 600–603 (2014).
43. J Fyfe, et al., Quantifying the influence of short-term emission reductions on climate. *Sci. Adv.* (in review).
44. GA McKinley, AR Fay, YA Eddebbar, L Gloege, NS Lovenduski, External forcing explains recent decadal variability of the ocean carbon sink. *AGU Adv.* **1**, e2019AV000149 (2020) e2019AV000149 2019AV000149.
45. AJ Turner, et al., Observed impacts of COVID-19 on urban CO_2 emissions. *Geophys. Res. Lett.* **47**, e2020GL090037 (2020).
46. Z Liu, et al., Carbon Monitor, a near-real-time daily dataset of global CO_2 emission from fossil fuel and cement production. *Sci. Data* **7** (2020).
47. KR Gurney, et al., The Vulcan version 3.0 high-resolution fossil fuel CO_2 emissions for the United States. *J. Geophys. Res. Atmospheres* **125** (2020).
48. K Gurney, B Mitra, P Dass, Y Song, T Moiz, Real-time U.S. fossil fuel carbon dioxide emissions: short and long-term impacts from the COVID-19 pandemic. *PNAS* **in review** (2020).
49. P Tans, R Keeling, Trends in atmospheric carbon dioxide (2020) https://www.esrl.noaa.gov/gmd/ccgg/trends/data.html, last accessed October 20, 2020.
50. RM Duren, et al., California's methane super-emitters. *Nature* **575**, 180–184 (2019).
51. A Thorpe, et al., Mapping methane concentrations from a controlled release experiment using the next generation airborne visible/infrared imaging spectrometer (AVIRIS-NG). *Remote. Sens. Environ.* **179**, 104–115 (2016).
52. S Claire, T Dinh, A Fanai, M Nguyen, S Schultz, Bay Area emissions: Inventory summary report: Greenhouse gases (2015) https://www.baaqmd.gov/~/media/Files/Planning%20and%20Research/Emission%20Inventory/BY2011_GHGSummary.ashx?la=en&la=en, last access 13 Nov 2020.
53. RB Jackson, et al., Increasing anthropogenic methane emissions arise equally from agricultural and fossil fuel sources. *Environ. Res. Lett.* **15**, 071002 (2020).
54. KW Bowman, Toward the next generation of air quality monitoring: Ozone. *Atmospheric Environ.* **80**, 571–583 (2013).
55. D Crisp, et al., A constellation architecture for monitoring carbon dioxide and methane from space (2018) http://ceos.org/document_management/Virtual_Constellations/ACC/Documents/CEOS_AC-VC_GHG_White_Paper_Publication_Draft2_20181111.pdf, last accessed 14 Nov 2020.
56. J Fishman, et al., Remote sensing of tropospheric pollution from space. *Bull. Am. Meteorol. Soc.* **89**, 805–822 (2008).
57. P Zoogman, et al., Tropospheric emissions: Monitoring of pollution (TEMPO). *J. Quant. Spectrosc. Radiat. Transf.* **186**, 17 – 39 (2017).
58. MG Kolm, et al., Sentinel 4: a geostationary imaging UVN spectrometer for air quality monitoring: status of design, performance and development in *International Conference on Space Optics — ICSO 2014*, eds. B Cugny, Z Sodnik, N Karafolas. (SPIE), (2017).
59. IN Polonsky, DM O'Brien, JB Kumer, CW O'Dell, the geoCARB Team, Performance of a geostationary mission, geoCARB, to measure CO_2, CH_4 and CO column-averaged concentrations. *Atmospheric Meas. Tech.* **7**, 959–981 (2014).
60. M Kasahara, et al., Overview and current status of GOSAT-GW mission and AMSR3 instrument in *Sensors, Systems, and Next-Generation Satellites XXIV*, eds. SP Neeck, T Kimura, A Hélière. (SPIE), (2020).
61. B Sierk, JL Bezy, A Loscher, Y Meijer, The European CO_2 Monitoring Mission: observing anthropogenic greenhouse gas emissions from space in *International Conference on Space Optics — ICSO 2018*, eds. N Karafolas, Z Sodnik, B Cugny. (SPIE), (2019).
62. R Nassar, et al., The Atmospheric Imaging Mission for Northern Regions: AIM-North. *Can. J. Remote. Sens.* **45**, 423–442 (2019).
63. D Fu, et al., Direct retrieval of isoprene from satellite-based infrared measurements. *Nat. Commun.* **10** (2019).
64. J Cuesta, et al., Transboundary ozone pollution across East Asia: daily evolution and photochemical production analysed by IASI + GOME2 multispectral satellite observations and models. *Atmospheric Chem. Phys.* **18**, 9499–9525 (2018).
65. P Ingmann, et al., Requirements for the GMES atmosphere service and ESA's implementation concept: Sentinels-4/-5 and -5p. *Remote. Sens. Environ.* **120**, 58–69 (2012).
66. AM Sayer, NC Hsu, J Lee, WV Kim, ST Dutcher, Validation, stability, and consistency of MODIS collection 6.1 and VIIRS version 1 deep blue aerosol data over land. *J. Geophys. Res. Atmospheres* **124**, 4658–4688 (2019).
67. MJ Garay, et al., Introducing the 4.4 km spatial resolution multi-angle imaging SpectroRadiometer (MISR) aerosol product. *Atmospheric Meas. Tech.* **13**, 593–628 (2020).
68. M Diao, et al., Methods, availability, and applications of PM2.5 exposure estimates derived from ground measurements, satellite, and atmospheric models. *J. Air & Waste Manag. Assoc.* **69**, 1391–1414 (2019).
69. MS Hammer, et al., Global estimates and long-term trends of fine particulate matter concentrations (1998–2018). *Environ. Sci. & Technol.* **54**, 7879–7890 (2020).
70. RA Kahn, BJ Gaitley, An analysis of global aerosol type as retrieved by MISR. *J. Geophys. Res. Atmospheres* **120**, 4248–4281 (2015).
71. DJ Diner, et al., Advances in multiangle satellite remote sensing of speciated airborne particulate matter and association with adverse health effects: from MISR to MAIA. *J. Appl. Remote. Sens.* **12**, 1 (2018).
72. RV Martin, et al., No one knows which city has the highest concentration of fine particulate matter. *Atmospheric Environ. X* **3**, 100040 (2019).
73. J Li, et al., Integrating low-cost air quality sensor networks with fixed and satellite monitoring systems to study ground-level PM2.5. *Atmospheric Environ.* **223**, 117293 (2020).
74. WW Sluis, MAF Allaart, AJM Piters, LFL Gast, The development of a nitrogen dioxide sonde. *Atmospheric Meas. Tech.* **3**, 1753–1762 (2010).
75. AA Shusterman, et al., The BErkeley Atmospheric CO_2 Observation Network: initial evaluation. *Atmospheric Chem. Phys.* **16**, 13449–13463 (2016).
76. J Kim, AA Shusterman, KJ Lieschke, C Newman, RC Cohen, The BErkeley Atmospheric CO_2 Observation Network: field calibration and evaluation of low-cost air quality sensors. *Atmospheric Meas. Tech.* **11**, 1937–1946 (2018).
77. N Zimmerman, et al., A machine learning calibration model using random forests to improve sensor performance for lower-cost air quality monitoring. *Atmospheric Meas. Tech.* **11**, 291–313 (2018).
78. N Zimmerman, et al., Improving correlations between land use and air pollutant concentrations using wavelet analysis: Insights from a low-cost sensor network. *Aerosol Air Qual. Res.* **20**, 314–328 (2020).
79. M Mead, et al., The use of electrochemical sensors for monitoring urban air quality in low-cost, high-density networks. *Atmospheric Environ.* **70**, 186–203 (2013).
80. I Heimann, et al., Source attribution of air pollution by spatial scale separation using high spatial density networks of low cost air quality sensors. *Atmospheric Environ.* **113**, 10–19 (2015).
81. OA Popoola, et al., Use of networks of low cost air quality sensors to quantify air quality in urban settings. *Atmospheric Environ.* **194**, 58–70 (2018).
82. R Tanzer-Gruener, J Li, SR Eilenberg, AL Robinson, AA Presto, Impacts of modifiable factors on ambient air pollution: A case study of COVID-19 shutdowns. *Environ. Sci. & Technol. Lett.* **7**, 554–559 (2020).
83. GG Pfister, et al., A MUlti-Scale Infrastructure for Chemistry and Aerosols - MUSICA. *Bull. Am. Meteorol. Soc.* **preprint**, 1–50 (2020).
84. J Flemming, et al., The CAMS interim reanalysis of carbon monoxide, ozone and aerosol for 2003–2015. *Atmospheric Chem. Phys.* **17**, 1945–1983 (2017).
85. K Miyazaki, KW Bowman, K Yumimoto, T Walker, K Sudo, Evaluation of a multi-model, multi-constituent assimilation framework for tropospheric chemical reanalysis. *Atmospheric Chem. Phys.* **20**, 931–967 (2020).
86. B Fasoli, JC Lin, DR Bowling, L Mitchell, D Mendoza, Simulating atmospheric tracer concentrations for spatially distributed receptors: updates to the Stochastic Time-Inverted Lagrangian Transport model's R interface (STILT-R version 2). *Geosci. Model. Dev.* **11**, 2813–2824 (2018).

DRAFT

PNAS
www.pnas.org

Supplementary Information for

The 2020 COVID-19 pandemic and atmospheric composition: back to the future

Joshua L. Laughner, Jessica L. Neu, David Schimel, Paul O. Wennberg, et al.

Full author list:
Joshua L. Laughner, Jessica L. Neu, David Schimel, Paul O. Wennberg, Kelley Barsanti, Kevin Bowman, Abhishek Chatterjee, Bart Croes, Helen Fitzmaurice, Daven Henze, Jinsol Kim, Eric A. Kort, Zhu Liu, Kazuyuki Miyazaki, Alexander J. Turner, Susan Anenberg, Jeremy Avise, Hansen Cao, David Crisp, Joost de Gouw, Annmarie Eldering, John Fyfe, Dan Goldberg, Kevin R. Gurney, Sina Hasheminassab, Francesca Hopkins, Cesunica E. Ivey, Dylan B.A. Jones, Nicole S. Lovenduski, Randall V. Martin, Galen A. McKinley, Lesley Ott, Benjamin Poulter, Muye Ru, Stanley P. Sander, Neil Swart, Yuk L. Yung, Zhao-Cheng Zeng, and the rest of the Keck Institute for Space Studies "COVID-19: Identifying Unique Opportunities for Earth System Science" study team

Corresponding Authors:
Joshua L. Laughner: jlaugh@caltech.edu
Jessica L. Neu: jessica.l.neu@jpl.nasa.gov
David Schimel: david.schimel@jpl.nasa.gov, or
Paul O. Wennberg: wennberg@gps.caltech.edu

This PDF file includes:

Supplementary text
Figs. S1 to S8
Tables S1 to S2
References for SI reference citations

Additional figures

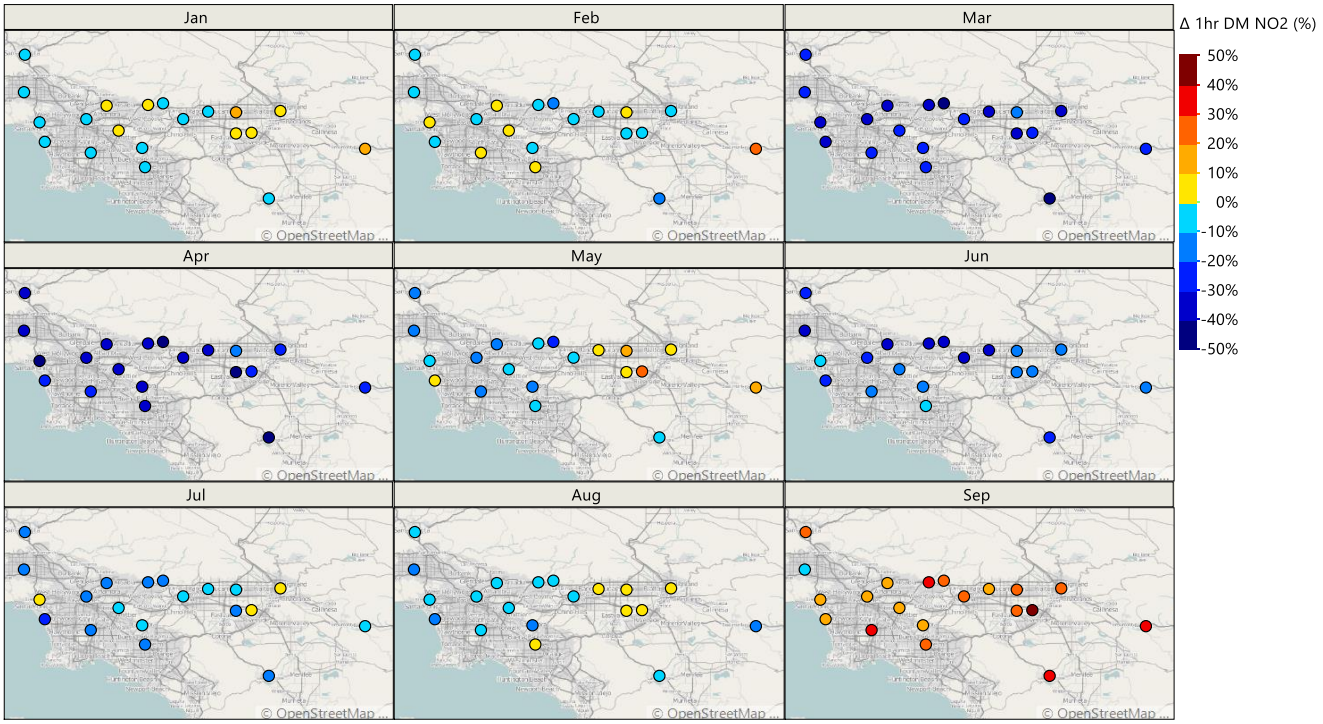

Fig. S1. Change in 1 hr daily maximum (DM) NO_2 in 2020 relative to the average of 2015 to 2019 at the California Air Resources Board sites throughout the South Coast Air Basin.

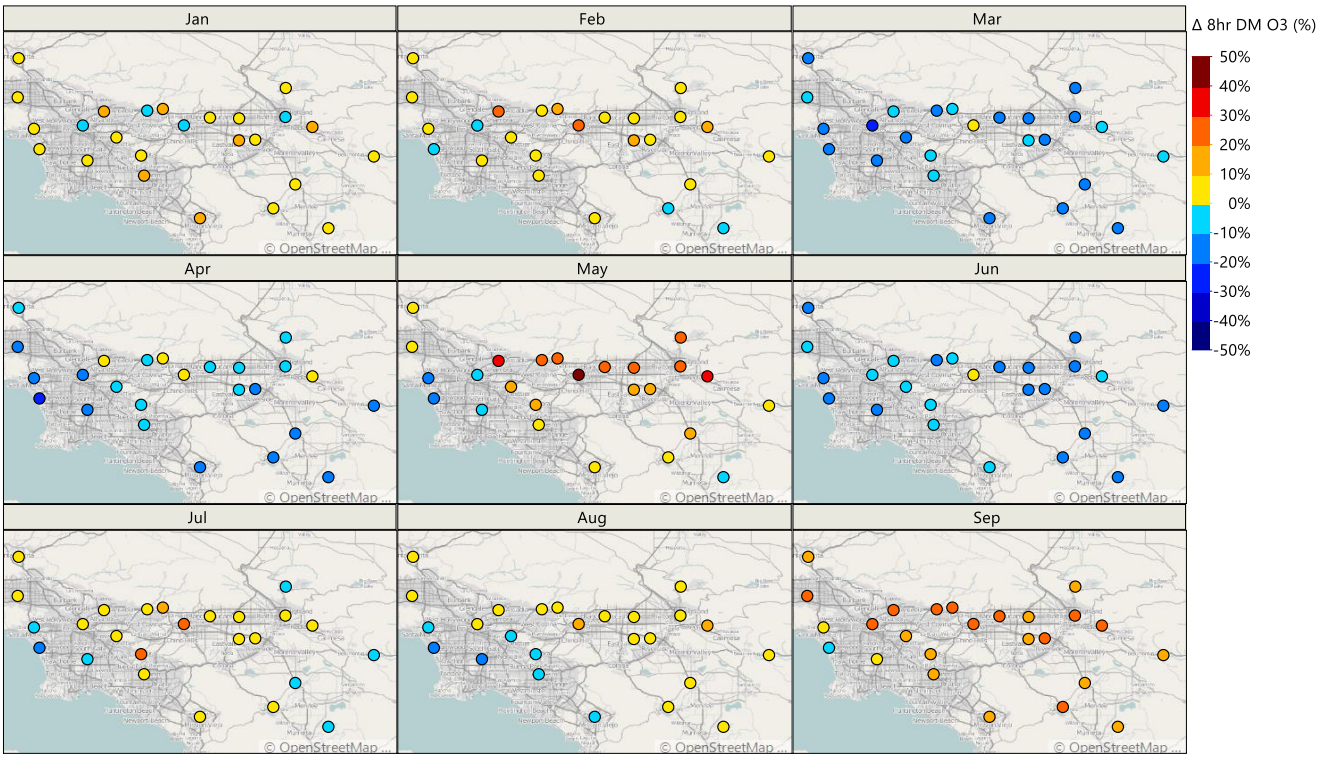

Fig. S2. Change in 8 hr daily maximum (DM) O_3 in 2020 relative to the average of 2015 to 2019 at the California Air Resources Board sites throughout the South Coast Air Basin.

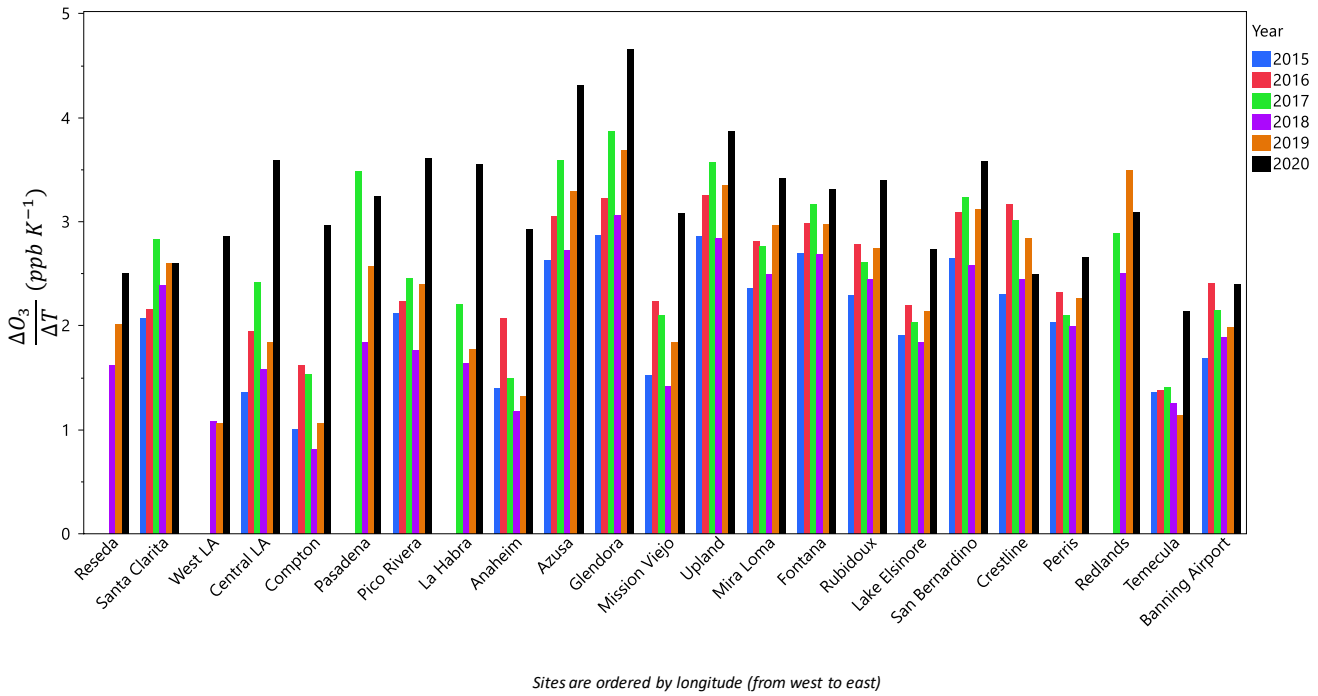

Fig. S3. Average derivatives of O_3 response vs. temperature between May and September at California Air Resources Board sites throughout the South Cost Air Basin for years 2015–2020. Each group of bars is one site, and are ordered by longitude (west to east).

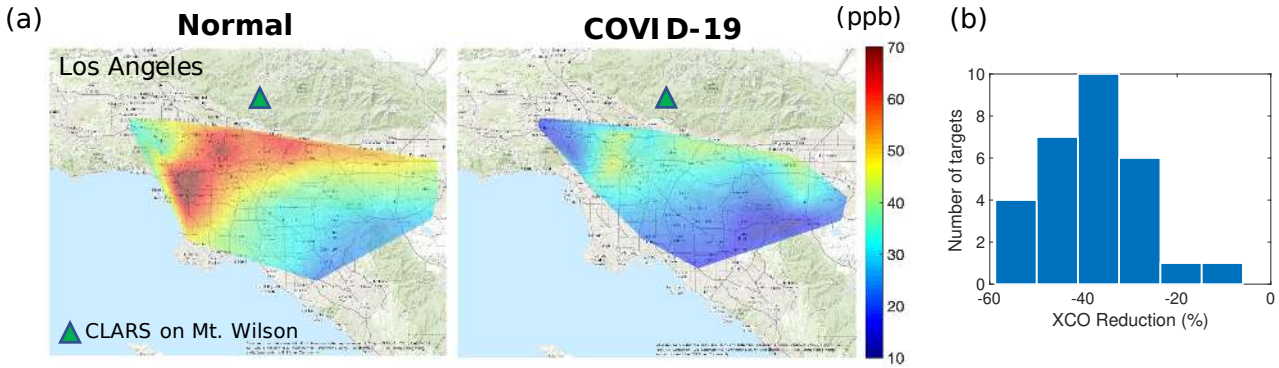

Fig. S4. (a) Maps of CO column abundance (XCO) in excess of the background in the Los Angeles (LA) basin averaged for the month of April. Left panel (Normal): April noontime average for 2012-2019. Right panel (COVID-19): April 2020 during lockdown. These maps are interpolated from the 33 surface observation targets by CLARS-FTS; **(b)** The histogram of difference between XCO excess measurements in (a) for all the surface observation targets. The averaged XCO excess reduction is 37.5% on average due to the lockdown order.

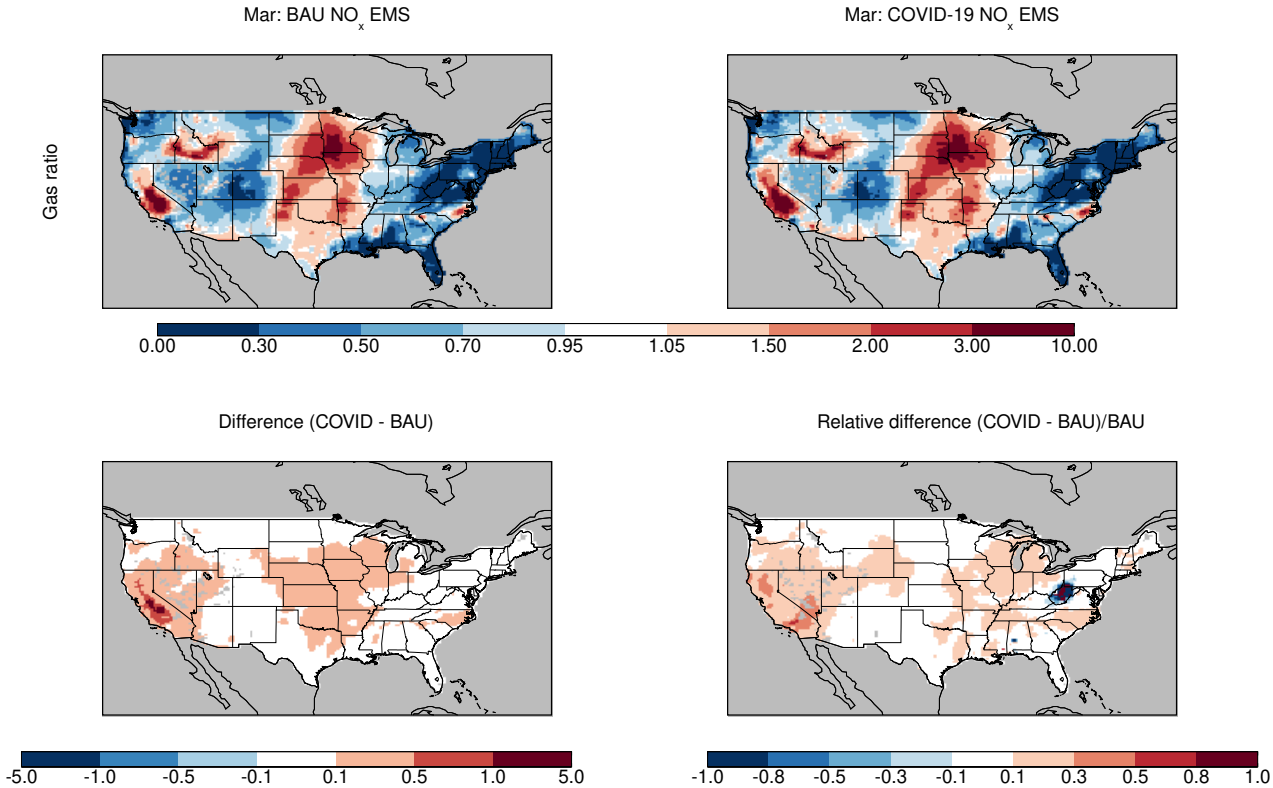

Fig. S5. Average change in gas ratios for March 2020 between a model simulation using business as usual (BAU) NO_x emissions and one using emissions based on NO_2 observations for March 2020 (COVID-19). The gas ratio is described in Eq. (1); a value < 1 indicates NH_3 limited nitrate aerosol formation; a value > 1 indicates NO_x limited aerosol formation.

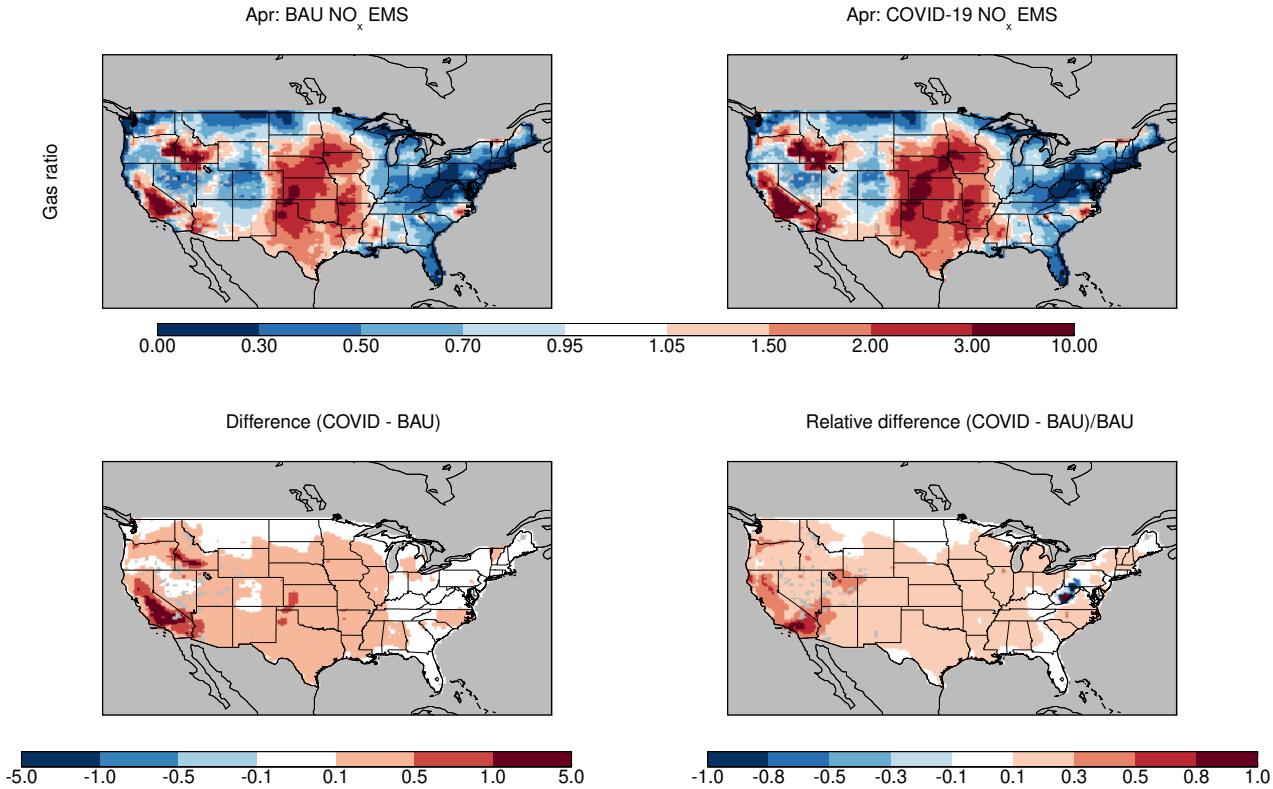

Fig. S6. Same as Fig. S7, but for April 2020.

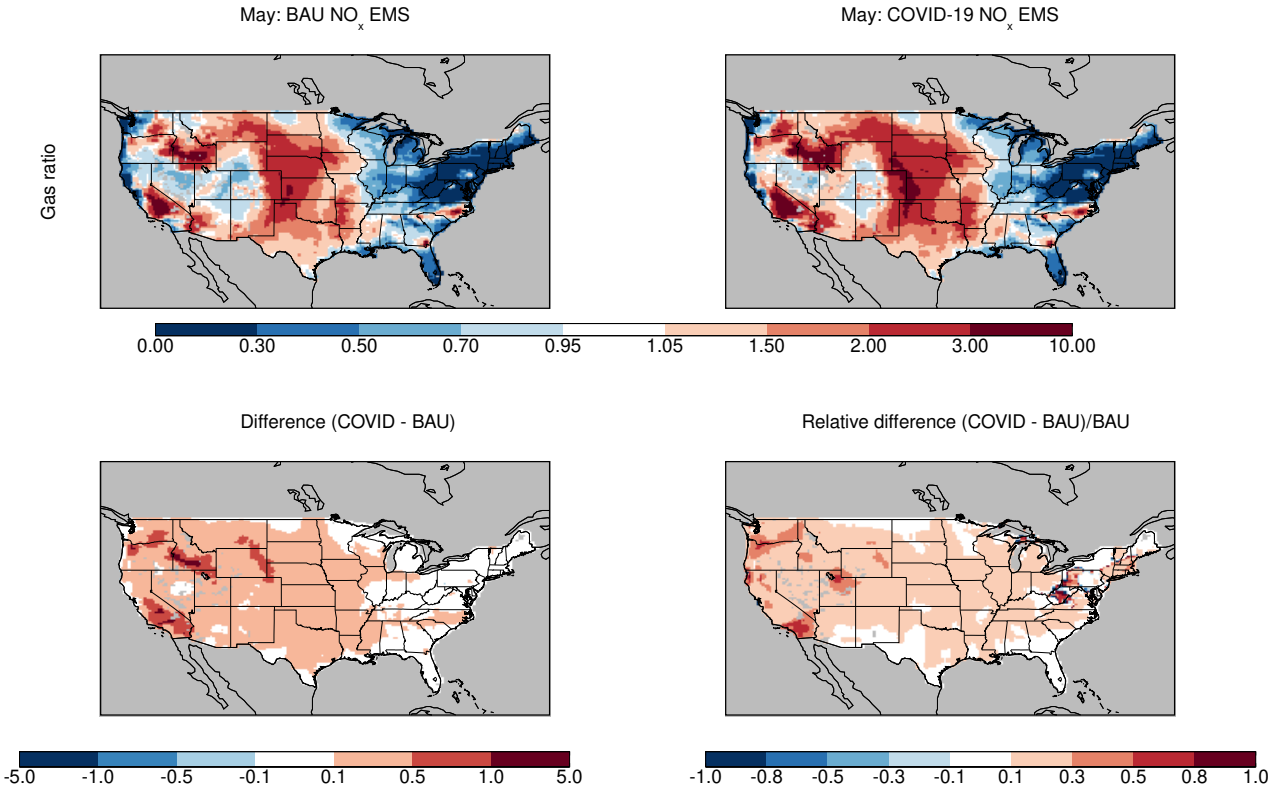

Fig. S7. Same as Fig. S7, but for May 2020.

Supporting Information Text

Methods

Public data. All public datasets used in this study are shown in Table S1.

Equivalent Emissions Year Calculations. For the CO_2 emissions in Fig.2a, we used 2005-2018 fossil fuel emissions from the Global Carbon Budget 2019 (12). For 2019, we assumed a +0.1% increase from 2018 based on Supplementary Data in Le Quere et al (13). For 2020 we used a 7% decrease from the 2019 value with a ± 1% uncertainty, based on Le Quere et al (13) and Liu et al (14). The 2020 emissions are 9.29 (± 0.10) GtC/yr; this corresponds to somewhere between 2010 (9.05 GtC/yr) and 2012 (9.50 GtC/yr). For CH_4, we use the anthropogenic emissions based on the EDGARv4.3.2 and GFED4.1s emissions inventories as published in the Global Methane Budget 2000-2017 (15). The emissions trajectory beyond 2017 is for illustrative purposes only and is not based on any data. For the global NO_x emission trajectory in Fig. 2 we used 2005-2020 emissions from the assimilation system described in the subsection "Global ozone production efficiency calculation" below. The equivalent year of 1999 ± 3.5 years was determined by applying the percent reduction between the average emissions over 2010-2014 and the 2020 emissions as determined by the assimilation system (-15.8%) to the 2010-2014 emissions from the CEDS and EDGAR5.0 inventories.

For Fig 2b, we again used the NO_x emissions from the assimilation system. For countries whose emissions have been monotonically increasing since 2005, we calculate the prior year with the same emissions as 2020. For countries whose emissions decreased over all or part of the 2005-2019 period, we use the 2015-2019 rate of decline to project emissions into the future.

Human activity metrics. The human activity metrics in Fig. 3 include the Oxford Coronavirus Government Response Index (1), Opensky-derived flight data (2, 16, 17), Port of LA container moves (https://www.portoflosangeles.org/business/statistics/container-statistics, last accessed 30 Oct 2020), Port of Oakland container moves (https://www.oaklandseaport.com/performance/facts-figures/, last accessed 30 Oct 2020), Caltrans PeMS daily vehicle counts (http://pems.dot.ca.gov/, last accessed 28 Oct 2020), Apple driving mobility data (https://covid19.apple.com/mobility, last accessed 28 Oct 2020), and U.S. Energy Information Agency electricity consumption (https://www.eia.gov/electricity/data/browser/#/topic/, last accessed 10 Aug 2020).

The CAADA Python package (18) was used to preprocess the PeMS vehicle counts and Strohmeier et al. (2) flight data, as well as download Port of LA and Port of Oakland container moves. For the purposes of Fig. 3, "Bay Area" is defined as Alameda, Contra Costa, Marin, San Mateo, San Francisco, Santa Clara, and Santa Cruz counties, while "LA" is defined as Los Angeles, Orange, Riverside, San Bernardino, Santa Barbara, and Ventura counties. For flight data, shipping data, and traffic data, daily values were normalized such that 15 Jan 2020 is 100% and monthly values were normalized such that Jan 2020 was 100%. For electricity use data, each month's value is the 2020 use as a percentage of 2019 use in the same month.

Dataset	Used for	Link	Last access	Citation
Oxford Stringency Index	Human activity metrics	https://www.bsg.ox.ac.uk/research/research-projects/coronavirus-government-response-tracker	11 Nov 2020	(1)
OpenSky-derived flight data	Human activity metrics	https://zenodo.org/record/3928564	11 Nov 2020	(2)
Port of Oakland container moves	Human activity metrics	https://www.oaklandseaport.com/performance/facts-figures/	11 Nov 2020	
Port of LA container moves	Human activity metrics	https://www.portoflosangeles.org/business/statistics/container-statistics	11 Nov 2020	
Port of Long Beach container moves	Human activity metrics	https://www.polb.com/business/port-statistics/#teus-archive-1995-to-present	10 Nov 2020	
Caltrans PeMS	Human activity & SF emissions	https://pems.dot.ca.gov/	11 Nov 2020	
Apple mobility trends	Human activity metrics	https://covid19.apple.com/mobility	27 Oct 2020	
US EIA electricity use	Human activity metrics	https://www.eia.gov/electricity/data/browser/#/topic/	10 Aug 2020	
CARB air quality data	LA Basin analysis	https://www.arb.ca.gov/aqmis2/aqdselect.php	11 Nov 2020	
OMI NO_2 columns	Global model assimilation (OPE)	http://www.qa4ecv.eu/ecv/no2-pre/data	11 Nov 2020	(3, 4)
TROPOMI NO_2 columns	Global model assimilation (OPE)	http://www.tropomi.eu/data-products/nitrogen-dioxide	11 Nov 2020	(5)
MOPITT CO	Global model assimilation (OPE)	https://www2.acom.ucar.edu/mopitt	11 Nov 2020	(6)
OMI SO_2 columns	Global model assimilation (OPE)	https://disc.gsfc.nasa.gov/datasets/OMSO2_003/summary	11 Nov 2020	(7, 8)
MLS O_3	Global model assimilation (OPE)	https://mls.jpl.nasa.gov/products/o3_product.php	11 Nov 2020	(9, 10)
MLS HNO_3	Global model assimilation (OPE)	https://mls.jpl.nasa.gov/products/hno3_product.php	11 Nov 2020	(9, 11)
BEACO2N CO_2 data	SF CO_2 emissions estimates	https://beacon.berkeley.edu/	11 Nov 2020	
NOAA HRRR meteorology	SF CO_2 emissions estimates	https://rapidrefresh.noaa.gov/hrrr/	11 Nov 2020	

Table S1. Public data sources used in this paper. The "Used for" column gives the part of the analysis in which that data was used.

TROPOMI NO_2 timeseries. For our analysis we re-grid the operational TROPOMI tropospheric vertical column NO_2, with native pixels of approximately 3.5×7 km^2 for 2019 and 3.5×5.5 km^2 for 2020, to a newly defined $0.01° \times 0.01°$ grid (approximately 1×1 km^2) centered over each of the three cities: Los Angeles, Lima, and Shanghai. Before re-gridding, the data are filtered so as to use only the highest quality measurements (quality assurance flag (QA_flag) > 0.75). By restricting to this QA value, we are removing mostly cloudy scenes (cloud radiance fraction > 0.5) and observations over snow-ice. Once the re-gridding has been completed, the data is binned temporally during a 15-day rolling timeframe and spatially over the metropolitan area, which we loosely define as a $1° \times 1°$ box over the city center. The rolling 75th percentile of the binned data during the first five months of 2019 annd 2020 are shown in top row of Figure 4. There is some evidence that the current TROPOMI operational NO_2 product may have a low bias of 20 to 40% in polluted areas; much of this bias may be attributed to the air mass factor (19–21). We limit our analysis to relative trends, which reduces this uncertainty.

LA Basin AQ analysis. The hourly ambient temperature and concentrations of PM2.5, NO_2, and O_3 in the South Coast Air Basin for the period of 1 Jan 2015 to 30 Sept 2020 were downloaded from the California Air Resources Board Air Quality Data Query Tool (https://www.arb.ca.gov/aqmis2/aqdselect.php). It should be noted that the 2020 data are preliminary, unvalidated, and subject to change. The following steps were taken for data analysis:

1. Only the monitoring sites that had complete data between 2015 and 2020 were considered in this analysis. Near-road monitoring sites were not included in the analysis. Figure S8 and Table S2 show the location of the monitoring sites considered in this analysis and the parameters measured at each site, respectively.

2. For every date and site, the 1hr daily maximum (DM) temperature, 24hr average PM2.5, 1hr DM NO_2, and 8hr average DM O_3 were calculated.

3. For every date, the average of the above-mentioned parameters was calculated across all monitoring sites. 7-day moving averages were then calculated and presented by day of year in Figure 4 for 2020 and the average ($\pm$ range) of [2015-2019]. The background colors in Figure 4 illustrate the difference between the 7-day moving average temperature in 2020 and the average ($\pm 1\sigma$) temperature in [2015-2019] by day of year.

4. Using the data in step 2, the percent change in monthly average concentrations of 1hr DM NO_2 and 8hr DM O_3 between 2020 and the average of [2015-2019] was calculated by month and site as shown in Figures S1 and S2.

Global ozone production efficiency calculation. We evaluated the seasonal and regional changes in the global tropospheric ozone response to COVID-19 NO_x emissions using a state-of-the-art chemical data assimilation system. Anthropogenic NO_x emission reductions linked to the COVID-19 pandemic were estimated as the difference between 2020 emissions and climatological (baseline) emissions for 2010-2019 estimated from our decadal chemical reanalysis constrained by multiple satellite measurements. The assimilation system uses the MIROC-CHASER global chemical transport model and an ensemble Kalman filter technique (22). This approach allows us to capture temporal and spatial variations in transport and chemical reactions in the emission and concentration estimates. The results for 2020 were used previously to evaluate the air quality response to Chinese COVID-19 lockdown (23), and show reasonable agreements with the observed concentrations from in-situ, ozonesonde, and satellite ozone measurements globally for 2005-2018 (23) as well as for 2020 (Miyazaki et al., paper in prep.).

In order to evaluate seasonal and regional differences in the ozone response, the ozone production efficiency (OPE) was estimated based on model sensitivity calculations using the 2020 and baseline emissions for February-July 2020. The OPE was calculated using the simulated global tropospheric ozone burden changes corresponding to changing NO_x emissions (i.e., the COVID-19 emission anomaly); the analysis was performed separately for each of the selected megacities. The model simulations were conducted from the beginning to the end of each month for the time period February to June, 2020, using the same initial conditions. The simulated tropospheric ozone burden averaged over the last 5 days of each month was compared between the simulations using the 2020 and baseline emissions. The analysis thus provides information on monthly changes in the ozone response (Tg) to reduced NO_x emissions (Tg per year) for each megacity separately.

PM2.5 simulations. We used the GEOS-Chem (v9-02) model with a bi-directional NH_3 flux scheme (24) at the nested resolution of $0.3125° \times 0.25°$ latitude to explore the sensitivity of inorganic aerosol formation to NO_x emission reductions in Los Angeles (118.239° W, 34.052° N) during COVID-19. Our detailed O_3-NO_x-VOC-aerosol simulations were driven by Goddard Earth Observing System (GEOS-FP 5.22.0) assimilated meteorological fields and include anthropgenic/biogenic/biomass burning emissions (25–27), gas-phase chemistry (28) and inorganic aerosol partitioning (29), wet/dry depositions (30–32) and transport. We first scaled anthropogenic NO_x and SO_2 emissions from HTAP v2 (25) (originally for the year 2010) to the year 2017 using satellite-derived SO_2 and NO_x emission reduction ratios (33) as our base emissions, which refer to emissions before lockdown during COVID-19. We scaled our base anthropogenic NO_x emissions in March by BAU/COVID monthly NO_x emission ratios from Miyazaki et al. (23) as our BAU/COVID emissions. In the COVID-19 simulations, the NO_x emissions started to decrease on March 1st.

We calculated the gas ratio (34) using Eq. (1):

$$\text{gas ratio} = \frac{[NH_3] + [NH_4^+] - 2[SO_4^{2-}]}{[HNO_3] + [NO_3^-]} \quad [1]$$

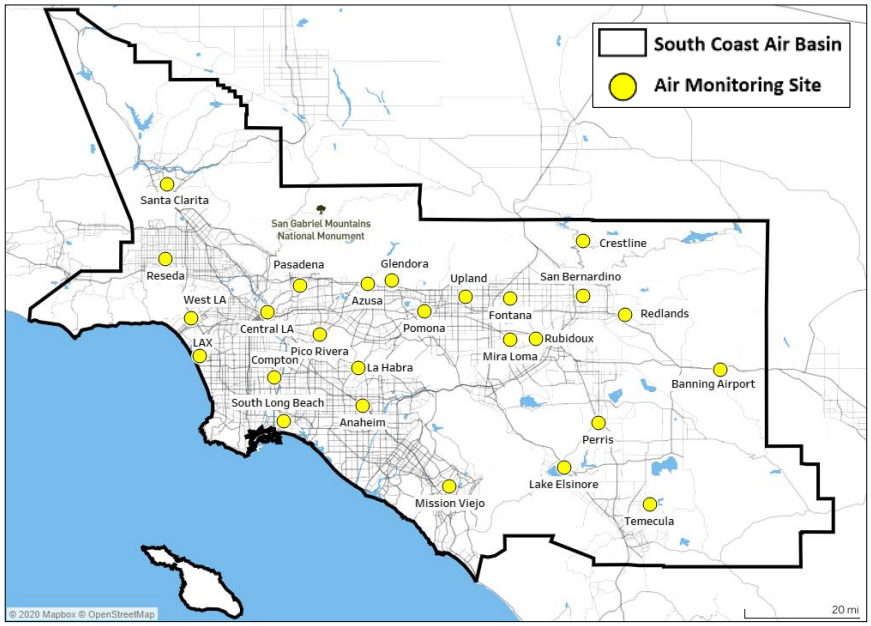

Fig. S8. Location of South Coast Air Basin monitoring sites included in this analysis.

Site	Temperature	O_3	PM2.5	NO_2
Anaheim	✓	✓	✓	✓
Azusa	✓	✓		✓
Banning airport	✓	✓	✓	✓
Central LA	✓	✓	✓	✓
Compton	✓	✓		✓
Crestline	✓	✓	✓	
Fontana	✓	✓		✓
Glendora	✓	✓	✓	✓
La Habra		✓		✓
Lake Elsinore	✓	✓	✓	✓
LAX		✓		✓
Mira Loma	✓	✓	✓	✓
Mission Viejo	✓	✓		
Pasadena		✓		✓
Perris	✓	✓		
Pico Rivera	✓	✓		✓
Pomona		✓		✓
Redlands		✓		
Reseda		✓	✓	✓
Rubidoux	✓	✓	✓	✓
San Bernadino	✓	✓		✓
Santa Clarita	✓	✓	✓	✓
South Long Beach			✓	
Upland	✓	✓	✓	✓
West LA		✓		✓
Temecula	✓	✓	✓	

Table S2. Parameters used from each South Coast Air Basin monitoring site.

$[NH_3]$, $[NH_4^+]$, $[SO_4^{2-}]$, $[HNO_3]$ and $[NO_3^-]$ are in units of molar concentrations (mol m^{-3}) and include both gas-phase and aerosol-phase. This gas ratio is an indicator of NH_4NO_3 production sensitivity to NO_x emission change and NH_3 emission change. Values > 1 indicate that NH_4NO_3 production is NO_x limited; values < 1 indicate it is NH_3 limited.

SF Bay Area CO_2 emissions estimates. To derive top-down emissions, Turner et al. (35) used 12 weeks of observational data from the BEACO$_2$N network (36) to estimate the most likely CO_2 fluxes from the San Francisco Bay Area before and during the shelter-in-place order (6 weeks of data before and 6 weeks of data during). Specifically, they estimated hourly fluxes at 900-m spatial resolution over the region and solved for posterior fluxes as:

$$\hat{\mathbf{x}} = \mathbf{x_a} + (\mathbf{HB})^T \left(\mathbf{HBH}^T + \mathbf{R}\right)^{-1} (\mathbf{y} - \mathbf{Hx_a}) \,. \qquad [2]$$

$\hat{\mathbf{x}}$ $(m \times 1)$ is the posterior emissions, $\mathbf{x_a}$ $(m \times 1)$ is the prior emissions, $\mathbf{y}$ $(n \times 1)$ is the BEACO$_2$N observations, $\mathbf{H}$ $(n \times m)$ is the matrix of footprints from HRRR-STILT, $\mathbf{R}$ $(n \times n)$ is the model-data mismatch error covariance matrix, and $\mathbf{B}$ $(m \times m)$ is the prior error covariance matrix.

Turner et al. (35) used meteorological fields from the NOAA High Resolution Rapid Refresh (HRRR), to drive the Stochastic Time-Inverted Lagrangian Transport (STILT) model, a Lagrangian particle dispersion model. Those trajectories were then used to construct measurement footprints ($\mathbf{H}$), representing the sensitivity of the measurement to a perturbation in emissions from a given location. Their prior emissions were adapted from previous work (37) with a biosphere derived from TROPOMI SIF observations (38). Upwind concentrations were taken from NOAA observations in the Pacific or AmeriFlux observations in California, depending on the endpoint of the back trajectory.

To derive bottom-up emissions, total hourly vehicle flow and percentage of trucks were retrieved from http://pems.dot.ca.gov from approximately 1800 traffic counting stations hosted by the Caltrans Performance Measurement System (PeMS) for January to June in 2019 and 2020. These sites encompass all highway sites within the 2020 footprint of the Berkeley Air Quality and CO_2 Network (BEACO$_2$N), as described in Turner et al. (35). These stations count vehicle flow using magnetic loops imbedded in roadways and estimate truck fraction using calculated vehicle speed and assumptions about vehicle length (39). For hours during which fewer than 50% of measurements were reported, we fill in total vehicle flow gaps by using linear fits to nearest neighbor sites and gaps in truck flow using hour-of-day-specific linear fits between neighboring sites. We calculate both car and truck vehicle miles traveled (VMT) for each highway segment during each hour using segment lengths obtained from the PeMS database. VMT for highway segments within the BEACO2N footprint are summed to obtain regional highway truck and car VMT for every hour. VMT is then converted to CO_2 using fleet estimates for fuel efficiency.

US CO_2 emissions estimates. Fuel consumption data from the U.S. Energy Information Administration (EIA) is used to generate weekly (Sat-Fri) estimates of FFCO_2 emissions between January 2005 and the week ending September 18, 2020. The input data includes all petroleum fuel consumption by fuel type, natural gas consumption by sector, and coal consumption by sector. These are organized into six fossil fuel consumption sectors: 1) gasoline-fueled transportation; 2) commercial surface transportation (i.e. land and water); 3) aviation; 4) electricity generation; 5) industrial energy consumption; and 6) residential/commercial energy consumption. Standard CO_2 emission factors are applied to the individual fuel types to achieve FFCO_2 emissions (40). To facilitate comparison to emission values in 2020, all time-series of FFCO_2 emissions are detrended. Comparison of weekly FFCO_2 emissions in 2020 are made to the long-term (2005 to 2019) weekly detrended median values and their associated 15-member ensemble distribution. Statistical significance is defined by departures that exceed a) the 1st/3rd quartile of the weekly ensemble distributions from 2005-2019, referred to as "partly significant" and b) the maximum/minimum distributions of the same weekly ensembles, referred to as "significant". The latter criteria are considered akin to a 2-sigma boundary for Gaussian statistics.

Global CO_2 growth rate simulations. The Goddard Earth Observing System (GEOS) is a flexible modeling and data assimilation system that has been widely used to study atmospheric composition and the carbon cycle (41). It includes the capability to simulate CO_2 concentrations in near real time by extrapolating previous year's biosphere and ocean fluxes (42). Here, we also include tracers that separately quantify the atmospheric impact of daily differences in fossil emissions between 2020 and 2019 using country-level estimates from Liu et al. (14) that are spatially disaggregated to ∼10-km using information from the Emissions Database for Global Atmospheric Research (43).

Global CO_2 emissions estimates. We calculated the daily global fossil CO_2 emissions in 2020 (updated to August 31st), as well as the daily sectoral emissions from power sector, industry sector, transport sector (including ground transport, aviation and shipping), and residential sector respectively. The estimates are based on a set of near real time dataset including hourly to daily electrical power generation data from national electricity operation systems of 31 countries, real-time mobility data (TomTom city congestion index data of 416 cities worldwide and FlightRadar24 individual flight location data), monthly industrial production data (calculated separately by cement production, steel production, chemical production and other industrial production of 27 industries) or indices (primarily Industrial Production Index) from national statistics of 62 countries/regions, and monthly fuel consumption data corrected for the daily population-weighted air temperature in 206 countries.

References

1. Hale T, et al. (2020) Oxford COVID-19 government response tracker. Blavatnik School of Government.

2. Strohmeier M, Olive X, Lübbe J, Schäfer M, Lenders V (2020) Crowdsourced air traffic data from the OpenSky network 2019–20. *Earth System Science Data Discussions* 2020:1–15.
3. Boersma KF, et al. (2017) QA4ECV NO_2 tropospheric and stratospheric column data from OMI. doi: 10.21944/QA4ECV-NO2-OMI-V1.1.
4. Boersma KF, et al. (2018) Improving algorithms and uncertainty estimates for satellite NO_2 retrievals: results from the quality assurance for the essential climate variables (QA4ECV) project. *Atmospheric Measurement Techniques* 11(12):6651–6678.
5. van Geffen J, et al. (2020) S5P TROPOMI NO_2 slant column retrieval: method, stability, uncertainties and comparisons with OMI. *Atmospheric Measurement Techniques* 13(3):1315–1335.
6. Deeter MN, et al. (2017) A climate-scale satellite record for carbon monoxide: the MOPITT Version 7 product. *Atmospheric Measurement Techniques* 10(7):2533–2555.
7. Krotkov NA, et al. (2016) Aura OMI observations of regional SO_2 pollution changes from 2005 to 2015. *Atmospheric Chemistry and Physics* 16(7):4605–4629.
8. Can Li, Nickolay A. Krotkov PL, Joiner J (2020) OMI/Aura Sulphur Dioxide (SO_2) Total Column 1-orbit L2 Swath 13x24 km V003, Greenbelt, MD, USA, Goddard Earth Sciences Data and Information Services Center (GES DISC). Accessed: 11 Nov 2020, doi: 10.5067/Aura/OMI/DATA2022.
9. Livesey NJ, et al. (2018) Earth Observing System (EOS) Aura Microwave Limb Sounder (MLS) Version 4.2x Level 2 and 3 data quality and description document (JPL D-33509 Rev. E). Available from, https://mls.jpl.nasa.gov/data/v4-2_data_quality_document.pdf, last access: 21 Nov 2020.
10. Schwartz M, Froidevaux L, Livesey N, Read W (2015) MLS/Aura Level 2 Ozone (O_3) Mixing Ratio V004, Greenbelt, MD, USA, Goddard Earth Sciences Data and Information Services Center (GES DISC). doi: 10.5067/Aura/MLS/DATA2017.
11. Manney G, Santee M, Froidevaux L, Livesey N, Read W (2015) MLS/Aura Level 2 Nitric Acid (HNO_3) Mixing Ratio V004, Greenbelt, MD, USA, Goddard Earth Sciences Data and Information Services Center (GES DISC). doi: 10.5067/Aura/MLS/DATA2012.
12. Friedlingstein P, et al. (2019) Global carbon budget 2019. *Earth System Science Data* 11(4):1783–1838.
13. Le Quéré C, et al. (2020) Temporary reduction in daily global CO_2 emissions during the COVID-19 forced confinement. *Nature Climate Change* 10(7):647–653.
14. Liu Z, et al. (2020) Near-real-time monitoring of global CO_2 emissions reveals the effects of the COVID-19 pandemic. *Nature Communications* 11(1).
15. Saunois M, et al. (2020) The global methane budget 2000–2017. *Earth System Science Data* 12(3):1561–1623.
16. Schäfer M, Strohmeier M, Lenders V, Martinovic I, Wilhelm M (2014) Bringing Up OpenSky: A Large-scale ADS-B Sensor Network for Research. *Proceedings of the 13th IEEE/ACM International Symposium on Information Processing in Sensor Networks (IPSN)* pp. 83–94.
17. Olive X (2019) traffic, a toolbox for processing and analysing air traffic data. *Journal of Open Source Software* 4(39).
18. Laughner J (2020) COVID Atmospheric Ancillary Data Agglomerator, v0.1.0.
19. Griffin D, et al. (2019) High-resolution mapping of nitrogen dioxide with TROPOMI: First results and validation over the Canadian oil sands. *Geophysical Research Letters* 46(2):1049–1060.
20. Judd LM, et al. (2020) Evaluating Sentinel-5P TROPOMI tropospheric NO_2 column densities with airborne and Pandora spectrometers near New York City and Long Island Sound. *Atmospheric Measurement Techniques* 13(11):6113–6140.
21. Verhoelst T, et al. (2020) Ground-based validation of the copernicus Sentinel-5p TROPOMI NO_2 measurements with the NDACC ZSL-DOAS, MAX-DOAS and Pandonia global networks. *Atmospheric Measurement Techniques Discussions* 2020:1–40.
22. Miyazaki K, et al. (2020) Updated tropospheric chemistry reanalysis and emission estimates, TCR-2, for 2005–2018. *Earth System Science Data* 12(3):2223–2259.
23. Miyazaki K, et al. (2020) Air quality response in China linked to the 2019 novel coronavirus (COVID-19) lockdown. *Geophysical Research Letters* 47(19):e2020GL089252. doi: 10.1029/2020GL089252.
24. Zhu L, et al. (2015) Global evaluation of ammonia bidirectional exchange and livestock diurnal variation schemes. *Atmospheric Chemistry and Physics* 15(22):12823–12843.
25. Janssens-Maenhout G, et al. (2015) HTAP_v2.2: a mosaic of regional and global emission grid maps for 2008 and 2010 to study hemispheric transport of air pollution. *Atmospheric Chemistry and Physics* 15(19):11411–11432.
26. Guenther AB, et al. (2012) The model of emissions of gases and aerosols from nature version 2.1 (MEGAN2.1): an extended and updated framework for modeling biogenic emissions. *Geoscientific Model Development* 5(6):1471–1492.
27. van der Werf GR, et al. (2010) Global fire emissions and the contribution of deforestation, savanna, forest, agricultural, and peat fires (1997–2009). *Atmospheric Chemistry and Physics* 10(23):11707–11735.
28. Mao J, et al. (2010) Chemistry of hydrogen oxide radicals (HO_x) in the arctic troposphere in spring. *Atmospheric Chemistry and Physics* 10(13):5823–5838.
29. Park RJ (2004) Natural and transboundary pollution influences on sulfate-nitrate-ammonium aerosols in the United States: Implications for policy. *Journal of Geophysical Research* 109(D15).
30. Liu H, Jacob DJ, Bey I, Yantosca RM (2001) Constraints from ^{210}Pb and ^{7}Be on wet deposition and transport in a global three-dimensional chemical tracer model driven by assimilated meteorological fields. *Journal of Geophysical Research: Atmospheres* 106(D11):12109–12128.

31. Wang Q, et al. (2011) Sources of carbonaceous aerosols and deposited black carbon in the arctic in winter-spring: implications for radiative forcing. *Atmospheric Chemistry and Physics* 11(23):12453–12473.
32. Amos HM, et al. (2012) Gas-particle partitioning of atmospheric Hg(II) and its effect on global mercury deposition. *Atmospheric Chemistry and Physics* 12(1):591–603.
33. Miyazaki K, et al. (2019) Chemical reanalysis products, doi: 10.25966/9qgv-fe81.
34. Ansari AS, Pandis SN (1998) Response of inorganic PM to precursor concentrations. *Environmental Science & Technology* 32(18):2706–2714.
35. Turner AJ, et al. (2020) Observed impacts of COVID-19 on urban CO_2 emissions. *Geophysical Research Letters* 47(22):e2020GL090037.
36. Shusterman AA, et al. (2016) The BErkeley atmospheric CO_2 observation network: initial evaluation. *Atmospheric Chemistry and Physics* 16(21):13449–13463.
37. Turner AJ, et al. (2016) Network design for quantifying urban CO_2: assessing trade-offs between precision and network density. *Atmospheric Chemistry and Physics* 16(21):13465–13475.
38. Turner AJ, et al. (2020) A double peak in the seasonality of California's photosynthesis as observed from space. *Biogeosciences* 17(2):405–422.
39. Kwon J, Varaiya P, Skabardonis A (2003) Estimation of truck traffic volume from single loop detectors with lane-to-lane speed correlation. *Transportation Research Record* 1856(1):106–117.
40. Gurney KR, et al. (2020) The Vulcan version 3.0 high-resolution fossil fuel CO_2 emissions for the United States. *Journal of Geophysical Research: Atmospheres* 125(19).
41. Ott LE, et al. (2015) Assessing the magnitude of CO_2 flux uncertainty in atmospheric CO_2 records using products from NASA's Carbon Monitoring Flux Pilot Project. *Journal of Geophysical Research: Atmospheres* 120(2):734–765.
42. Weir B, et al. (2020) Calibrating satellite-derived carbon fluxes for retrospective and near real-time assimilation systems.
43. Crippa M, et al. (2020) High resolution temporal profiles in the emissions database for global atmospheric research. *Scientific Data* 7(1).